

**PRODUCTION OF BIO-JET FUEL FROM PALM FATTY ACID
DISTILLATE OVER TEOS-MODIFIED NiPd/ZSM-5 CATALYSTS**

Umbon Boonsard

A Thesis Submitted in Partial Fulfillment of the Requirements
for the Degree of Master of Science
The Petroleum and Petrochemical College, Chulalongkorn University
in Academic Partnership with
The University of Michigan, The University of Oklahoma,
and Case Western Reserve University
2021



3782235724

CU Theses 6271009063 thesis / recv: 13092564 11:18:12 / seq: 50



3782235724

Production of Bio-jet Fuel from Palm Fatty Acid Distillate over TEOS-modified NiPd/ZSM-5 Catalysts

Miss Umbon Boonsard

A Thesis Submitted in Partial Fulfillment of the Requirements
for the Degree of Master of Science in Petrochemical Technology
Common Course
The Petroleum and Petrochemical College
Chulalongkorn University
Academic Year 2020
Copyright of Chulalongkorn University



378235724

CU ThesIs 6271009063 thesis / recv: 13092564 11:18:12 / seq: 50

การสังเคราะห์น้ำมันไบโอดีเซลจากกรดไขมันปาล์มโดยใช้ตัวเร่งปฏิกิริยานิกเกิลแพลเลเดียมบนตัว
รองรับซีโอไลต์ซีเอสเอ็ม 15 ที่ปรับปรุงด้วยทีอีโอเอส

น.ส.อุ้มบุญ บุญศาสตร์

วิทยานิพนธ์นี้เป็นส่วนหนึ่งของการศึกษาตามหลักสูตรปริญญาวิทยาศาสตรมหาบัณฑิต
สาขาวิชาเทคโนโลยีปิโตรเคมี ไม่สังกัดภาควิชา/เทียบเท่า
วิทยาลัยปิโตรเลียมและปิโตรเคมี จุฬาลงกรณ์มหาวิทยาลัย
ปีการศึกษา 2563
ลิขสิทธิ์ของจุฬาลงกรณ์มหาวิทยาลัย



378235724

CU Thesisis 6271009063 thesis / recv: 13092564 11:18:12 / seq: 50

อุ้มบุญ บุญศาสตร์: การสังเคราะห์น้ำมันไบโอเจ็ทจากกรดไขมันปาล์มโดยใช้ตัวเร่งปฏิกิริยานิกเกิลแพลเลเดียม บนตัวรองรับซีโอไลต์ซีเอสเอ็มไฟว์ที่ปรับปรุงด้วยทีอีโอเอส. (Production of Bio-jet Fuel from Palm Fatty Acid Distillate over TEOS-modified NiPd/ZSM-5 Catalysts)

อ. ที่ปรึกษาหลัก : รศ. ดร.ศิริพร จงผาคัญ

เชื้อเพลิงเจ็ทส่วนใหญ่ได้มาจากการกลั่นน้ำมันดิบปิโตรเลียม ซึ่งส่งผลกระทบต่อสิ่งแวดล้อมโดยการปล่อยแก๊สเรือนกระจก ดังนั้นการพัฒนาเชื้อเพลิงไบโอเจ็ทจึงเป็นสิ่งที่น่าสนใจในอุตสาหกรรมการบิน หนึ่งในวัตถุดิบทางเลือกที่นำมาพัฒนาเป็นน้ำมันไบโอเจ็ทคือ กรดไขมันปาล์มเนื่องจากมีต้นทุนค่อนข้างต่ำ โดยกรดไขมันปาล์มสามารถเปลี่ยนไปเป็นน้ำมันไบโอเจ็ทโดยผ่านปฏิกิริยาไดออกซิเดชัน ไอโซเมอไรเซชัน และแครกกิง ในงานวิจัยนี้ตัวเร่งปฏิกิริยาโลหะนิกเกิลแพลเลเดียม (NiPd) บนตัวรองรับซีเอสเอ็มไฟว์ (ZSM-5) ที่อัตราส่วนซิลิกอนต่ออะลูมิเนียมแตกต่างกัน (23, 50, และ 280) และปรับปรุงตัวรองรับซีเอสเอ็มไฟว์ (ZSM-5) ด้วยทีอีโอเอส (TEOS) จะถูกทดสอบด้วย XRD, BET, XRF, XPS และ TEM หลังจากปรับปรุงตัวรองรับซีเอสเอ็มไฟว์ (ZSM-5) ด้วยทีอีโอเอส (TEOS) พบว่ามีซิลิกอน (Si) อยู่บนผิวภายนอกของตัวรองรับซีเอสเอ็มไฟว์ (ZSM-5) เพิ่มขึ้น นอกจากนี้ตัวเร่งปฏิกิริยาที่ปรับปรุงด้วยทีอีโอเอส (TEOS) แสดงให้เห็นว่ามีโครงสร้างและการกระจายตัวของโลหะนิกเกิลและแพลเลเดียม (Ni and Pd) ที่คล้ายคลึงกับตัวเร่งปฏิกิริยา ก่อนการปรับปรุง นอกจากนี้ตัวเร่งปฏิกิริยาได้ถูกทดสอบโดยใช้เครื่องปฏิกรณ์แบบเบดนิ่งชนิดไหลต่อเนื่อง จากผลการทดลองพบว่า NiPd/ZSM-5 (23) มีความเป็นกรดสูงส่งผลให้เกิดผลิตภัณฑ์เบามาก NiPd/ZSM-5 (280) มีความเป็นกรดต่ำส่งผลให้เกิดปฏิกิริยาไฮโดรแครกกิงได้น้อยทำให้เกิดผลิตภัณฑ์ดีเซลสูง NiPd/ZSM-5 (50) สามารถผลิตน้ำมันไบโอเจ็ทได้ร้อยละ 27.1 ซึ่งมากกว่า NiPd/ZSM-5 (23) และ NiPd/ZSM-5 (280) (ร้อยละ 22.8 และ ร้อยละ 21.7 ตามลำดับ) เนื่องจากมีความเป็นกรดที่เหมาะสมต่อการแตกตัวของไฮโดรคาร์บอนสายโซ่ยาวให้อยู่ในช่วงของน้ำมันไบโอเจ็ท นอกจากนี้ตัวเร่งปฏิกิริยาที่ปรับปรุงด้วยทีอีโอเอส (TEOS) สามารถเพิ่มการผลิตน้ำมันไบโอเจ็ทและลดการเกิดผลิตภัณฑ์เบาเมื่อเปรียบเทียบกับตัวเร่งปฏิกิริยาที่ไม่ได้ปรับปรุง ดังนั้น TEOS-NiPd/ZSM-5 (50) สามารถผลิตน้ำมันไบโอเจ็ทได้มากที่สุด ร้อยละ 44.2 และมีอัตราส่วนสายโซ่กิ่งต่อสายโซ่ตรงในช่วง C₉-C₁₄ เท่ากับ 1.65 ภายใต้อุณหภูมิที่เหมาะสมที่อุณหภูมิ 350 องศาเซลเซียส ความดัน 30 บาร์ สัดส่วนสารป้อนต่อปริมาณตัวเร่งปฏิกิริยา 1.5 ต่อชั่วโมง และสัดส่วนไฮโดรเจนต่อสารตั้งต้นเท่ากับ 8

สาขาวิชา เทคโนโลยีปิโตรเคมี
ปีการศึกษา 2563

ลายมือชื่อนิสิต
ลายมือชื่อ อ.ที่ปรึกษาหลัก

6271009063 : MAJOR PETROCHEMICAL TECHNOLOGY

KEYWOR Bio-jet fuel/ PFAD/ ZSM-5/ Nikel/ Palladium/ Deoxygenation/
D: Isomerization/ Hydrocracking

Umbon Boonsard : Production of Bio-jet Fuel from Palm Fatty Acid
Distillate over TEOS-modified NiPd/ZSM-5 Catalysts. Advisor: Assoc.
Prof. SIRIPORN JONGPATIWUT, Ph.D.

Jet fuels are mainly derived from the refining of petroleum feedstock which has a negative impact to the environment as it emits greenhouse gases (GHG). Therefore, the development of an alternative and renewable jet fuel is an imminent concern of the aviation industry. One of the alternative jet fuel feedstocks is palm fatty acid distillate (PFAD) due to its relatively low cost. Bio-jet fuel can be produced via three reactions including deoxygenation, isomerization, and cracking. In this study, the bimetallic NiPd supported on ZSM-5 with various Si/Al ratios (23, 50, and 280) and modified ZSM-5 by TEOS were characterized by XRD, BET, XRF, XPS, and TEM. After TEOS modification, the Si on the external surface of ZSM-5 zeolites was increased. Moreover, the TEOS-modified ZSM-5 catalyst showed similar morphological structure and bimetallic (Ni and Pd) dispersion as the unmodified catalyst. In addition, the prepared catalysts were tested in a continuous flow fixed bed reactor. NiPd/ZSM-5 (23) had high acidity, resulting in high light products. NiPd/ZSM-5 (280) exhibited a low acidity, resulting in low hydrocracking, giving high diesel product. NiPd/ZSM-5 (50) had a higher bio-jet fuel yield of 27.1% as compared to NiPd/ZSM-5 (23) and NiPd/ZSM-5 (280) (22.8% and 21.7%, respectively) due to its suitable acidity for cracking long-chain hydrocarbon into the range of bio-jet. Moreover, TEOS-modified catalyst gave higher bio-jet fuel yield with a lower light product as compared to the unmodified catalyst. Thus, TEOS-NiPd/ZSM-5 (50) exhibited the maximum bio-jet fuel yield of 44.2% with an *i-/n*-paraffin ratio (C₉-C₁₄) of 1.65 under the optimum reaction condition at 350 °C, 30 bar, LHSV of 1.5 h⁻¹, and H₂/feed molar ratio of 8.

Field of Study:	Petrochemical Technology	Student's Signature
	
Academic	2020	Advisor's Signature
Year:	

ACKNOWLEDGEMENTS

First, I am deeply grateful to my thesis advisor, Assoc. Prof. Siriporn Jongpatiwut for her supervision, suggestion, and encouragement throughout this research. This thesis would not have been completely finished without her precious advice and supports.

I would like to express my sincere thank to Prof. Thirasak Rirksomboon and Prof. Tawan Sooknoi for being my committee and their suggestion which are certainly important and helpful for the completion of this thesis.

I would like to thank all faculty and staff at The Petroleum and Petrochemical College, Chulalongkorn University for their kind assistance and cooperation.

I am thankful to my seniors, Ms. Yanika Sangasang and Ms. Jarujit Chaowichitra for their suggestions, advice, encouragement, and help me modified the pipeline system.

Moreover, I would like to thank all of my PPC friends, especially Ms. Somluk Sanorkham, Ms. Warissara Angurawanich, Ms. Orawee Champadang, Ms. Kawinna Tookjit, Ms. Nareerat Hanka, and Mr. Supanut Charoenkiatkong for all supports and encouragement in my hard time.

Finally, I would like to express my deepest thanks to my parent for their love, supports, and encouragement since I was young until completing this project.

Umbon Boonsard

TABLE OF CONTENTS

	Page
ABSTRACT (THAI)	iii
ABSTRACT (ENGLISH).....	iv
ACKNOWLEDGEMENTS	v
TABLE OF CONTENTS.....	vi
LIST OF TABLES	ix
LIST OF FIGURES	xi
CHAPTER 1 INTRODUCTION	1
CHAPTER 2 THEORETICAL BACKGROUND AND LITERATURE REVIEW.....	3
2.1 Jet Fuel.....	3
2.2 Bio-jet Fuel	4
2.3 Vegetable Oil	5
2.4 Fatty Acid	6
2.5 Palm Fatty Acid Distillate Feedstock	7
2.6 Reaction Pathway of Deoxygenation.....	11
2.6.1 Hydrogenation	12
2.6.1.1 β -Elimination.....	12
2.6.1.2 γ -Hydrogen Transfer.....	13
2.6.2 Deoxygenation.....	13
2.6.2.1 Decarboxylation (DCO ₂).....	14
2.6.2.2 Decarbonylation (DCO)	14
2.6.2.3 Hydrodeoxygenation (HDO).....	15
2.6.3 Cracking and Isomerization Reactions.....	16
2.6.3.1 Hydrocracking	17
2.6.3.2 Hydroisomerization	18
2.7 The Catalyst for Biofuel Production.....	19

2.7.1 Zeolite as a Catalyst for Bio-jet Fuel Production	20
2.7.2 Active Metal and Promoter	22
2.7.3 Chemical Liquid Deposition (CLD).....	23
CHAPTER 3 METHODOLOGY	25
3.1 Materials and Equipment	25
3.2 Experimental Procedures	26
3.2.1 Catalyst Preparation	26
3.2.1.1 Chemical Liquid Deposition (CLD).....	26
3.2.2 Metal Loading on Zeolite Support	27
3.3 Catalyst Characterization.....	27
3.3.1 X-ray Diffraction (XRD).....	27
3.3.2 Brunauer-Emmett-Teller (BET).....	27
3.3.3 Transmission Electron Microscopy (TEM).....	28
3.3.4 X-ray Fluorescence Spectrometry (XRF).....	28
3.3.5 X-ray Photoelectron Spectroscopy (XPS).....	28
3.4 Catalyst Activity Testing	29
3.5 Product Analysis.....	31
3.5.1 Liquid Products Analysis	31
3.5.2 Gas Product Analysis	32
CHAPTER 4 RESULTS AND DISCUSSION.....	33
4.1 Characterization of Catalysts.....	33
4.1.1 X-ray Diffraction (XRD).....	33
4.1.2 Brunauer-Emmett-Teller (BET)	34
4.1.3 Chemical Composition	36
4.1.4 Transmission Electron Microscopy (TEM).....	37
4.2 Gas Chromatography of Feed and Standard Analysis.....	39
4.2.1 Feed Analysis	39
4.2.2 Standard Analysis.....	40
4.3 Catalytic Activity Testing.....	42

4.3.1 Effect of the Si/Al Ratios (23, 50, and 280).....	42
4.3.2 Effect of TEOS Modification on ZSM-5 Zeolites.....	45
4.3.3 Effect of Reaction Temperature	46
4.3.4 Effect of Reaction Pressure	47
4.4 The Proposed Reaction Pathway	48
CHAPTER 5 CONCLUSIONS AND RECOMMENDATIONS	49
5.1 Conclusion	49
5.2 Recommendation	49
APPENDICES	50
Appendix A Graphical Abstract	50
Appendix B1 Overall Mass Balance of Deoxygenation-hydroprocessing over NiPd/ZSM-5 with Various Si/Al Ratio (23, 50, and 280).....	51
Appendix B2 Overall Mass Balance of Deoxygenation-hydroprocessing at TEOS modification on ZSM-5 Zeolites	53
Appendix B3 Overall Mass Balance of Deoxygenation-hydroprocessing at Different in Temperature	55
Appendix B4 Overall Mass Balance of Deoxygenation-hydroprocessing at Different in Pressure	57
REFERENCES	59
VITA	62

LIST OF TABLES

	Page
Table 2.1 The general production pathways of synthesized paraffinic kerosene (SPK) (Yang, Xin et al. 2019)	5
Table 2.2 Chemical structure for common vegetable oil of fatty acid (Lestari, Mäki-Arvela et al. 2009).....	7
Table 2.3 General properties of PFAD (Kapor, Maniam et al. 2017).....	11
Table 2.4 Price of crude palm oil and PFAD in Malaysia for October 2018 (Ceic, 2021)	11
Table 3.1 Description of system in flow diagram of the continuous flow fixed bed reactor	30
Table 3.2 The reaction conditions for hydroprocessing of palm fatty acid distillate in continuous flow fixed bed reactor	31
Table 3.3 The chromatographic temperature program for liquid product analysis.....	32
Table 3.4 The chromatographic temperature program for gas-phase product analysis	33
Table 4.1 Physical characteristics of the prepared catalysts analyzed by BET.....	35
Table 4.2 Chemical composition of the prepared catalysts analyzed by XRF.....	37
Table 4.3 Si/Al ratio of the prepared catalysts analyzed XPS and XRF.....	37
Table 4.4 Composition of PFAD feedstock	40
Table B1 Overall mass balance of deoxygenation-hydroprocessing one-pot reaction over NiPd/ZSM-5 (23), NiPd/ZSM-5 (50), and NiPd/ZSM-5 (280) catalysts (Reaction condition: 350 °C, 30 bar, LHSV of 1.5 h ⁻¹ , H ₂ /feed molar ratio of 8, and TOS = 3) .51	51
Table B2 Overall mass balance of deoxygenation-hydroprocessing one-pot reaction over NiPd/ZSM-5 (23), TEOS-NiPd/ZSM-5 (23), TEOS(2)-NiPd/ZSM-5 (23) NiPd/ZSM-5 (50), TEOS-NiPd/ZSM-5 (50), NiPd/ZSM-5 (280), and TEOS-NiPd/ZSM-5 (280) catalysts (Reaction condition: 350 °C, 30 bar, LHSV of 1.5 h ⁻¹ , H ₂ /feed molar ratio of 8 and TOS = 3 h)	53
Table B3 Overall mass balance of deoxygenation-hydroprocessing one-pot reaction over TEOS-NiPd/ZSM-5 (50) catalyst in different temperature (Reaction condition: 30 bar, LHSV of 1.5 h ⁻¹ , H ₂ /feed molar ratio of 8 and TOS = 3 h)	55



37828295724

CU IThesis 6271009063 thesis / rev: 13092564 11:18:12 / seq: 50

Table B4 Overall mass balance of deoxygenation-hydroprocessing one-pot reaction over NiPd/SiO₂-ZSM-5 (50) catalyst in different pressure (Reaction condition: 350 °C, LHSV of 1.5 h⁻¹, H₂/feed molar ratio of 8 and TOS = 3 h)57



378235724

CU Theses 6271009063 thesis / recv: 13092564 11:18:12 / seq: 50

LIST OF FIGURES

	Page
Figure 2.1 Typical structure of a triglyceride molecule (Ong et al., 2011).	6
Figure 2.2 Reaction of glycerol and fatty acids to produce triglyceride, which is constituent of vegetable oil (Lestari, Mäki-Arvela et al. 2009).	6
Figure 2.3 Oil palm tree and fruits (Ong, Mahlia et al. 2011).	8
Figure 2.4 Fresh oil palm fruit image with its longitudinal section (Foo and Hameed 2009).	8
Figure 2.5 World palm oil production in 2009 (Ong, Mahlia et al. 2011).	9
Figure 2.6 Physical refining process of crude palm oil (Kiatkittipong, Phimsen et al. 2013).	10
Figure 2.7 Plausible deoxygenation pathways of triglycerides (Rai and Da Silva 2017).	12
Figure 2.8 Dominant pathways in the thermal cracking of triglyceride determined by (a) β -elimination and (b) γ -hydrogen transfer (Khan, Lup et al. 2019).	13
Figure 2.9 The possible deoxygenation pathways (Mohammad, Hari et al. 2013). ...	14
Figure 2.10 Decarboxylation and decarbonylation of (a) tristearin and (b) stearin acid (Pattanaik and Misra 2017).	15
Figure 2.11 Hydrodeoxygenation reaction scheme for model compounds of triglycerides and fatty acids (a) tristearin and (b) stearic acid with thermodynamic data (Pattanaik and Misra 2017).	16
Figure 2.12 The schematic of hydrocracking reaction (Fahim, Al-Sahhaf et al. 2009).	17
Figure 2.13 Mechanism of n-paraffins/n-alkanes hydroisomerization over bifunctional catalysts using n-decane as a model compound (Galadima. and Muraza., 2015).	18
Figure 2.14 Oligomeric silicate and alumino-silicate species can form structural units or building blocks, which subsequently organize to give different zeolite structures (Ramsay and Kallus 2000).	21
Figure 3.1 The schematic diagram of the reactor system.	30
Figure 4.1 XRD patterns of the prepared catalysts.	34
Figure 4.2 N ₂ adsorption and desorption isotherms of the prepared catalysts.	35

Figure 4.3 TEM images of (a) parent ZSM-5 (50), (b) NiPd/ZSM-5 (50), and (c) TEOS-NiPd/ZSM-5 (50).....	39
Figure 4.4 The chromatogram of various components in PFAD analyzed by a GC/FID.	40
Figure 4.5 Chromatograms of standard oxygenated compounds.....	41
Figure 4.6 Chromatograms of standard n-alkanes.	41
Figure 4.7 PFAD conversion and product yield over (a) NiPd/ZSM-5 (23), (b) NiPd/ZSM-5 (50), and (c) NiPd/ZSM-5 (280) (Reaction condition: 350°C, 30 bar, LHSV = 1.5 h ⁻¹ , and H ₂ /feed = 8).	43
Figure 4.8 PFAD conversion, product yield, and iso-/n-paraffin (C ₉ -C ₁₄) over NiPd/ZSM-5 (23), NiPd/ZSM-5 (50), and NiPd/ZSM-5 (280) (Reaction condition: 350°C, 30 bar, LHSV = 1.5 h ⁻¹ , H ₂ /feed =8 and TOS = 3 h).	44
Figure 4.9 PFAD conversion, product yield, and iso-/n-paraffin (C ₉ -C ₁₄) over NiPd/ZSM-5 (23), TEOS-NiPd/ZSM-5 (23), TEOS (2)-NiPd/ZSM-5 (23), NiPd/ZSM-5 (50), TEOS-NiPd/ZSM-5 (50), NiPd/ZSM-5 (280), and TEOS-NiPd/ZSM-5 (280) catalysts (Reaction condition: 350 °C, 30 bar, LHSV = 1.5 h ⁻¹ , H ₂ /feed = 8 and TOS = 3 h).	46
Figure 4.10 PFAD conversion, product yield, and iso-/n-paraffin ratio (C ₉ -C ₁₄) over TEOS-NiPd/ZSM-5 (50) with different temperature (Reaction condition: 30 bar, LHSV = 1.5 h ⁻¹ , H ₂ /feed molar ratio of 8 and TOS = 3 h).	47
Figure 4.11 PFAD conversion, product yield, and iso-/n-paraffin ratio (C ₉ -C ₁₄) over TEOS-NiPd/ZSM-5 (50) with different pressure (Reaction condition: 350 °C, LHSV = 1.5 h ⁻¹ , H ₂ /feed molar ratio of 8 and TOS = 3 h).	48
Figure 4.12 The proposed reaction pathway of bio-jet fuel production from palmitic acid over bi-functional catalysts.	50
Figure A.1 Graphical Abstract.....	50

CHAPTER 1

INTRODUCTION

The global aviation industry is expected to grow due to the increasing industrialization and modernization. The most commercial and military aviation fuel are mainly derived from the refining of petroleum feedstock. Conversely, the petroleum-based aviation fuel has a negative impact on the environment, mainly through the emission of green-house gas (GHG). Hence, the development of an alternative and renewable jet fuel is an imminent concern of scientists and the aviation industry to saving the environment and reducing GHG emission (Zhang, Hui, *et al.*, 2016).

One of the alternative jet fuels feedstocks is vegetable oil. Vegetable oils are mainly composed of triglycerides containing various saturated and unsaturated fatty acids (Ong *et al.*, 2011). The fatty acids present in vegetable oil which are considered as one of the most attractive model compounds that can be used in large scale for production of hydrocarbon fuels. Palm is one of the alternative resources for biofuel production. Palm fatty acid distillate (PFAD) is a by-product from in the deodorization of crude palm oil and normally used in soap and oleochemical industries. PFAD is a potential feedstock for renewable fuels due to its low price (Kiatkittipong *et al.*, 2013).

Bio-jet fuel can be produced from fatty acid via deoxygenation (DO) reaction such as hydrodeoxygenation (HDO), decarboxylation (DCO₂), and decarbonylation (DCO) to remove oxygen in the fatty acid molecules and hydroprocessing, which involves hydrogenation, hydrocracking, and isomerization. Bifunctional catalyst is come into consideration to convert PFAD into saturated paraffins in the range of jet fuels (C₉-C₁₄) (Mohammad *et al.*, 2013). The TEOS-modified NiPd/ZSM-5 with different Si/Al ratios of 23, 50 and 280 have been studied in this work. Pd is a noble metal highly active to deoxygenation process (De Lucas *et al.*, 2006). Ni is a non-noble metal exhibiting high efficiency in deoxygenation process at high reaction pressure. ZSM-5 catalysts are widely used in the petroleum and petrochemical industry because of their acid properties, high hydrothermal stability, hydrocracking,



3782235724

CU IThesis 6271009063 thesis / rev: 13092564 11:18:12 / seq: 50

and isomerization. However, the high acidity, especially at external surface of ZSM-5 results in undesired cracking product, giving a low bio-jet fuel selectivity. Therefore, the decreased of external Brønsted acid over ZSM-5 zeolites by chemical liquid deposition (CLD) has been investigated.

In this study, the production of bio-jet fuels from PFAD was investigated in a continuous flow fixed bed reactor. The bimetallic NiPd supported on ZSM-5 with various Si/Al ratios (23, 50, and 280) were prepared by incipient wetness impregnation. Moreover, the TEOS-modified NiPd/ZSM-5 catalysts were prepared by chemical liquid deposition (CLD) method to tailor the external surface of ZSM-5 by SiO₂. The catalysts were used to investigate the conversion and product selectivity during the catalyst activity testing. The catalysts were characterized by X-ray diffractometer (XRD), X-ray fluorescence spectrometry (XRF), X-ray photoelectron spectroscopy (XPS), Brunauer-Emmett-Teller (BET) surface area analyzer, and transmission electron microscopy (TEM). Moreover, the optimum operating condition (i.e., temperature and pressure) for the production of bio-jet fuel was also investigated.



378235724

CHAPTER 2

THEORETICAL BACKGROUND AND LITERATURE REVIEW

2.1 Jet Fuel

Jet fuel is a type of aviation fuel designed for use in aircraft powered by gas-turbine engines. It is clear to straw-colored in appearance. Jet fuel is multi-component fuel which is the mixture of paraffins, naphthenes or cycloparaffins with a typical chain-length distribution of C₆-C₁₆ (Kallio *et al.*, 2014). The major component is n-paraffins, iso-paraffins, and cycloparaffins or naphthenes (approximately 70-85%) which are mainly responsible for reducing the freezing point of jet fuel. The aromatics are present less than 25%. The aromatic contents have the impact on the fuel's anti-oxidation properties and lubricity. However, high aromatic content may lead to smoke formation which can damage the combustion chamber (Blakey *et al.*, 2011) The most used jet fuel are the kerosene-type fuels which are Jet A and Jet A-1. Both of Jet A and Jet A-1 are used in commercial airplane. Jet A fuel is generally used in the United States, While Jet A-1 is adopted in the rest of the world. The different between Jet A and Jet A-1 is the freezing point which are 40 °C and 47 °C respectively (Zhang, Hui, *et al.*, 2016).

Aviation produces the same type of emission as other ground transportation vehicles, including carbon monoxide (CO), carbon dioxide (CO₂), water vapor (H₂O), nitrogen oxide (NO_x), sulfur oxide (SO_x), unburned hydrocarbon (UHC) and particulate matters (PM) depending on whether the occur near the ground or at altitude, aircraft emission can be considered as greenhouse gas (GHG) that can be the primary of the climate change. With the concerns about its environmental impacts and the fossil issue, alternative jet fuel derived from non-conventional sources become an important strategy achieving a sustainable and green aviation (Zhang, Hui, *et al.*, 2016).

2.2 Bio-jet Fuel

The global aviation industry is expected to be increasing due to the increased industrialization, modernization and development have to high demand worldwide. Global energy consumption in 2008 is growing almost double consumption from 1980 which is 11,295 million tons of oil equivalent (Mtoe) and 6,630 Mtoe respectively (Ong *et al.*, 2011). The large consumption of jet fuel also generated considerable greenhouse gas (GHG) emissions. In Every year, jet fuel release 2% global CO₂ emission. The aviation industries have a purpose to achieve a 50% reduction in CO₂ emission by 2050 as compared to 2005. Bio-based aviation Fuel (bio-jet fuel) have a great interest as alternative for conventional jet fuels. The International Air Transport Association (IATA) has identified bio-jet fuel as the most promising strategy to reduce CO₂ emissions from the aviation sector in the future (Yang *et al.*, 2019).

Table 2.1 shows the general production pathways certified synthesized paraffinic kerosene (SPK). Five types of SPK as blending components for conventional jet fuel (in certain volume percentage) have defined by American Society for Testing and Material (ASTM) D7566-18.

Table 2.1 The general production pathways of synthesized paraffinic kerosene (SPK) (Yang, Xin et al. 2019)

Pathway	SPK	Descriptions
Gas-to-jet	FT-SPK	Gasification to obtain Syn-gas (CO + H ₂); Fisher-Tropsch (FT) to synthesize paraffins and olefins, followed by hydroprocessing
	FT-SPK/A	In addition to the FT-SPK, the aromatic content is intentionally increased by adding alkylated and bio-based aromatics.
Oil-to-jet	HEFA-SPK	Deoxygenation of mono-, di- and triglycerides, free fatty acids, and fatty acid esters, followed by hydroprocessing
Sugar-to-jet	SIP-SPK	Hydrolysis to obtain fermentable sugar; fermentation of sugars for farnesene production, follow by hydroprocessing and fractionation
Alcohol-to-jet	ATJ-SPK	Hydrolysis to obtain fermentable sugars; fermentation of sugars for iso-butanol and ethanol production, followed by dehydration, oligomerization, hydrogenation, and fractionation

2.3 Vegetable Oil

The vegetable oil was used as a fuel around 100 years ago by the inventor of diesel engine. After exploration of fossil fuels, they were continued to be major conventional energy source. With the increasing trend of industrialization and modernization the world energy demand is also increasing at a faster rate (Malvade and Satpute, 2013) Vegetable oil have the chemical structure that shown in **Table 2.1** comprise of 98% triglyceride and small amounts of mono and diglyceride. Vegetable oil contains fatty acid, free fatty acid, phospholipids, phosphatides, carotenes, tocopherols, Sulphur compound and traces of water (Ong *et al.*, 2011).

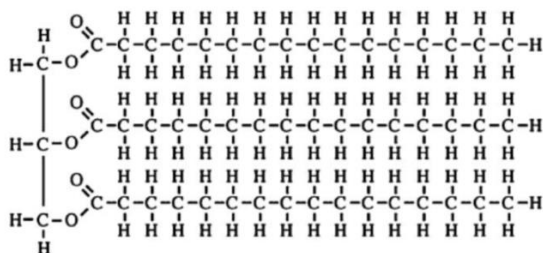


Figure 2.1 Typical structure of a triglyceride molecule (Ong et al., 2011).

As shows in **Figure 2.2** a triglyceride is the reaction product of one glycerol with three fatty acid molecules. The fatty acids vary in their carbon chain and number of unsaturated chains (Lestari *et al.*, 2009)

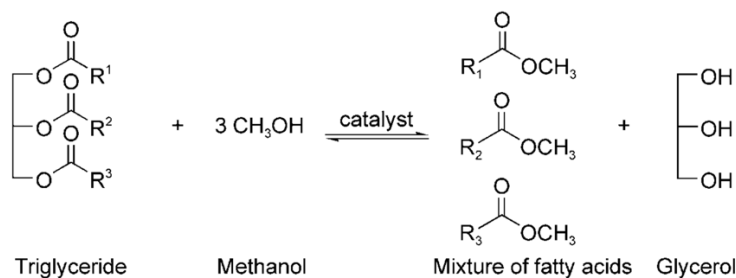


Figure 2.2 Reaction of glycerol and fatty acids to produce triglyceride, which is constituent of vegetable oil (Lestari, Mäki-Arvela et al. 2009).

2.4 Fatty Acid

Fatty acid that commonly found in vegetable oil are stearic acid, palmitic, oleic, linoleic, linolenic and the summary of the fatty acid composition of some common vegetable oil as shown in **Table 2.2**. Vegetable oil can be used as liquid engine fuel in various ways such as straight vegetable oil, oil blends, pyrolysis, micro-emulsification, and transesterification in diesel engine (Ong *et al.*, 2011).

Table 2.2 Chemical structure for common vegetable oil of fatty acid (Lestari, Mäki-Arvela et al. 2009)

Trivial name	IUPAC name	Structure x:y ^[a]	M _r	m.p. [°C]	b.p [°C (kPa)]
Saturated					
Capric acid	Decanoic acid	10:0	172.3	32	239.7 (101.3)
Lauric acid	Dodecanoic acid	12:0	200.3	43	20.6 (101.3)
Myristic acid	Tetradecanoic acid	14:0	228.3	54	298.9 (101.3)
Palmitic acid	Hexadecanoic acid	16:0	256.3	62	309.0 (68.3)
Stearic acid	Octadecanoic acid	18:0	284.5	69	332.6 (68.3)
Arachidic acid	Eicosanoic acid	20:0	312.5	75	355.2 (68.3)
Behenic acid	Docosanoic acid	22:0	340.6	81	-
Monounsaturated					
Palmitoleic acid	9-hexadecenoic acid	16:1	254.4	0	-
Oleic acid	9-octadecenoic acid	18:1	282.5	13	334.7 (53.3)
Vaccenic acid	11-octadecenoic acid	18:1	282.5	7	-
Gadoleic acid	9-eicosenoic acid	20:1	310.5	25	-
Erucic acid	13-docosenoic acid	22:1	338.6	33	-
Polyunsaturated					
Linoleic acid	9,12-octadecadienoic acid	18:2	280.5	-9	230.0 (2.1)
A-linoleic acid	9,12,15-octadecatrienoic acid	18:3	278.4	-17	230.0 (2.3)
A-linolenic acid	6,9,12-octadecatrienoic acid	18:3	278.4	-	-
Arachidonic acid	5,8,11,14-eicosatetraenoic acid	20:4	304.5	-50	-
EPA	5,8,11,14,17-eicosapentaenoic acid	20:5	302.4	-	-

[a] Number of carbon atom (x) and number of unsaturated bonds (y)

2.5 Palm Fatty Acid Distillate Feedstock

Oil palm is botanical classification as *Elaeis guineensis* and native to the West Africa where it was growing wild and later developed into agricultural crop. The oil palm is a tropical plant and grow well in lowland with humidity that shown in **Figure 2.3**. The fruitlet consists of a fibrous mesocarp layer and endocarp (shell) containing the kernel (endosperm) which contain oil and carbohydrate reserve for the embryo as shown in **Figure 2.4** (Foo. and Hameed., 2009). The world production of

palm oil is 45 million tons and highest production in South East Asia with a total 89% of total palm oil production as shown in **Figure 2.5** (Ong *et al.*, 2011).



Figure 2.3 Oil palm tree and fruits (Ong, Mahlia et al. 2011).

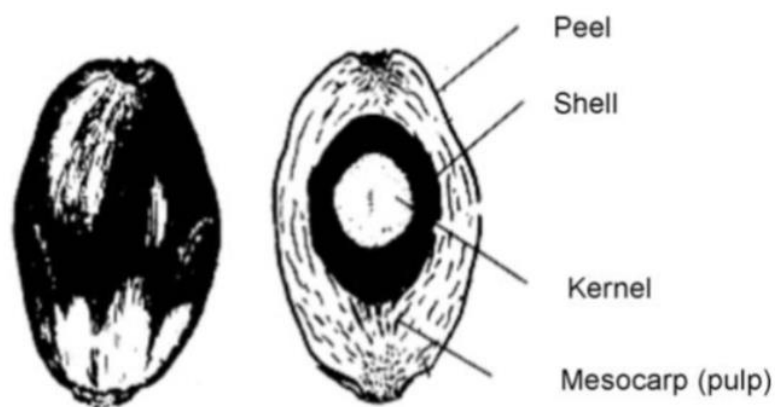


Figure 2.4 Fresh oil palm fruit image with its longitudinal section (Foo and Hameed 2009).

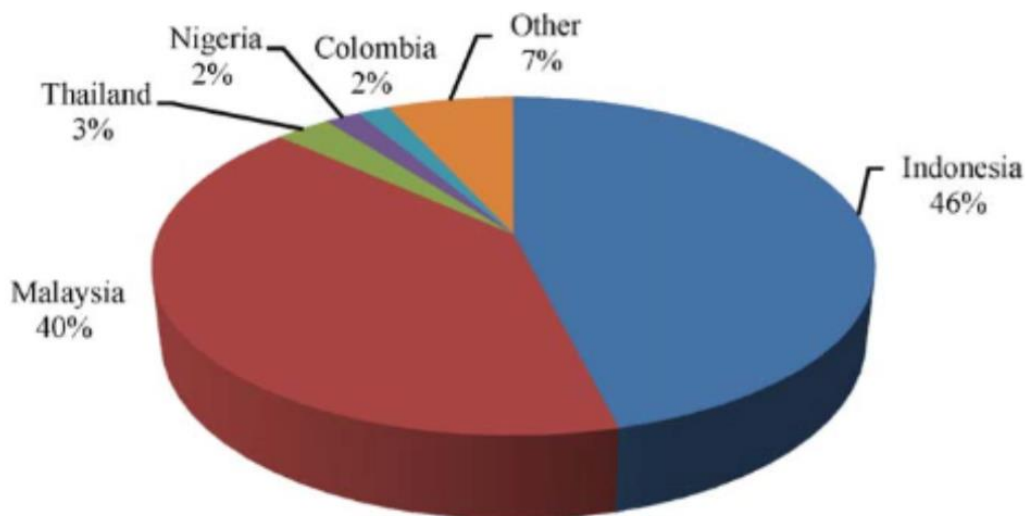


Figure 2.5 World palm oil production in 2009 (Ong, Mahlia et al. 2011).

Palm fatty acid distillate (PFAD) is a by-product from palm oil refinery which is generated in the deodorization. **Figure 2.6** shows the physical refining process of crude palm oil. The crude palm oil (CPO) is physically refined by removing impurity to the acceptable level. Firstly, an impurity call gum (phospholipids, phosphatides) in CPO was removed by precipitation process. This process occurs at 90-130 °C and uses phosphoric acid as a precipitant. At this state, degummed palm oil (DPO) is obtained. The DPO is then bleached to remove any undesirable impurities such as pigment and trace metal, giving a bleached palm oil (BPO). Next, the BPO is deodorized to eliminate free fatty acid content. This step gives refined, bleached, deodorized palm oil (RBDPO) and palm fatty acid distillate (PFAD) as a by-product. Finally, the RBDPO is fractionated to yield refined palm olein and refined palm stearin. It should be noted that PFAD was successfully employed as a starting material to produce H₂ via steam reforming and methyl ester in near-critical methanol condition (Kiatkittipong *et al.*, 2013).

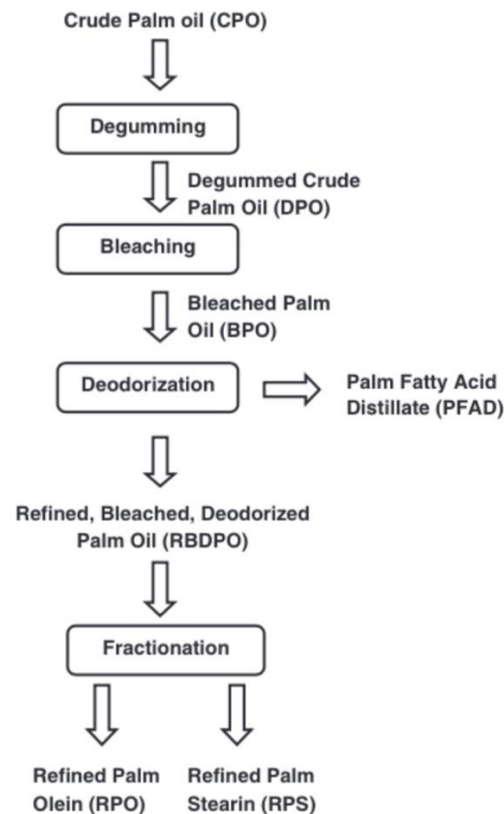


Figure 2.6 Physical refining process of crude palm oil (Kiatkittipong, Phimsen et al. 2013).

PFAD is light brown semi solid at room temperature and melts to brown liquid when higher temperature is applied. PFAD consists of more than 80% free fatty acid with palmitic acid and oleic acid as main components. **Table 2.3** shows the general properties of PFAD from previous study. Compared to other refined oil that being used currently as feedstock in the most biodiesel plant, the price of PFAD is much lower. **Table 2.4** shows the price of PFAD with comparison with CPO in Malaysia for October 2018 (Ceic, 2021). It found that the PFAD price is lower than CPO. The price of PFAD is cheaper than other refined oil which are major feed stocks for most of current biofuel plant.

Table 2.3 General properties of PFAD (Kapor, Maniam et al. 2017)

Properties	(Ping. and Yusof., 2009)	(Lokman <i>et al.</i> , 2015)
FFA content (as palmitic, %)	72.7-92.6	86.3 ± 1.75
Iodine value, (gI ₂ /100g)	46.3-57.6	
Saponification value (mg KOH/g)	200.3-251.4	149.74 ± 4.72
Unsaponifiable matter (%)	1.0-2.5	
Moisture content (%)	0.03-0.24	0.089 ± 0.004
Tire (°C)	46.0-48.3	
Fatty acid composition (wt%)		
C _{14:0}	0.9-1.6	1.9 ± 0.05
C _{16:0}	43.0-49.1	45.7 ± 1.32
C _{18:0}	4.0-4.5	4.3 ± 0.09
C _{18:1}	34.7-37.2	40.2 ± 1.21
C _{18:2}	8.5-9.7	7.9 ± 0.21

Table 2.4 Price of crude palm oil and PFAD in Malaysia for October 2018 (Ceic, 2021)

	Price (MYR/Ton)
Crude palm oil (CPO)	2,084.500
Palm fatty acid distillate (PFAD)	1,489.000

2.6 Reaction Pathway of Deoxygenation

Normally, the main component of lipid biomass consists of triglycerides, which are divided into two part which is glycerol and fatty acid. Fatty acid has a carbon chain length from 14 to 30 atom depending on the source of the biomass. To produce paraffin with the same length (C_n) or one atom shorter (C_{n-1}). There are three proposed decomposition pathways (1) β-elimination, (2) γ-hydrogen transfer, and (3) direct deoxygenation pathways as shows in **Figure 2.7** (Rai and Da Silva, 2017).

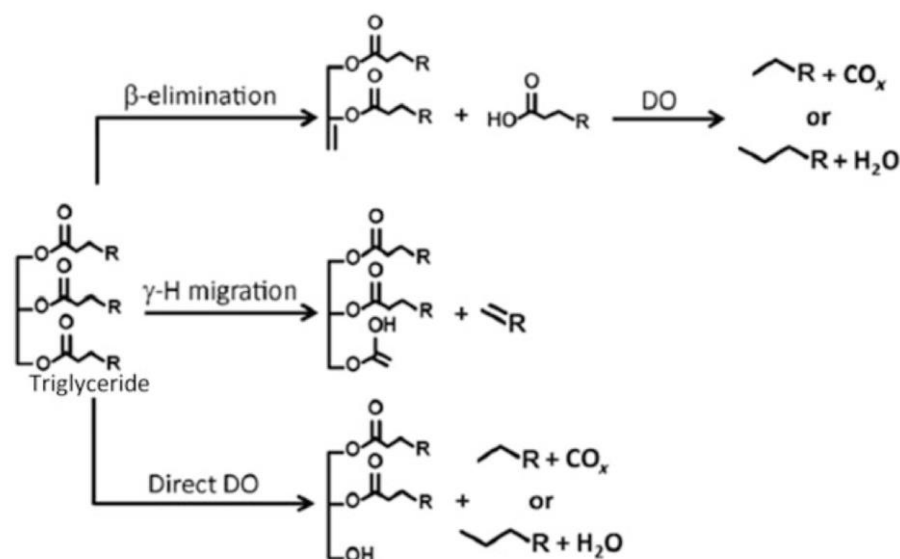


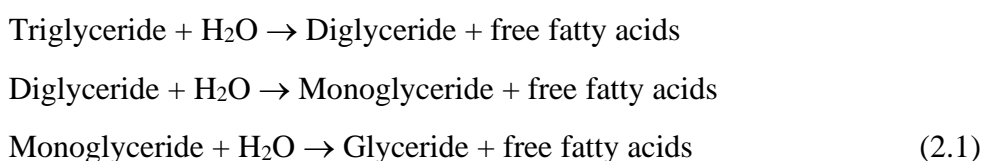
Figure 2.7 Plausible deoxygenation pathways of triglycerides (Rai and Da Silva 2017).

2.6.1 Hydrogenation

Hydrogenation of triglyceride-based feedstock involves the addition of two hydrogen atoms to unsaturated double bonds (C=C) in the fatty acid in H_2 pressurized to transform into saturated hydrocarbon. The leading pathway hydrogenation/hydrolysis of triglyceride is combined with β -elimination and γ -hydrogen transfer.

2.6.1.1 β -Elimination

β -elimination process is a process that releasing one fatty acid of triglyceride under H_2 pressure produces fatty acid (carboxylic acid) and unsaturated glycol di-fatty ester/diglycerides that shown in **Figure 2.8**. Moreover, hydrogenation of diglycerides through β -elimination forms a negligible extent of monoglycerides in the form of palmitic acid (C16:0), stearic acid (C18:0) and arachidic acid (C20:0) as intermediate products. However, the major of the monoglycerides were converted into free fatty acid (FFA) and glycerol. A complete set of reaction mechanism of triglyceride to free fatty acid id giving in Eq.2.1 (Khan *et al.*, 2019).



2.6.1.2 γ -Hydrogen Transfer

The cleavage of C-C bond in the alkyl group by and transformation of the terminal olefin with two carbons lesser (C_{n-2}) than the original fatty acid chain as shown in **Figure 2.8**. During hydrogenation, fatty acid yield might gradually decrease, and hydrocarbon yield may increase in the form of alkanes or α -olefins. This process gaseous products are not expected, and only stable saturated fatty acids were formed. These results confirmed that the fatty acids are indeed the intermediate product of triglyceride and no extra double bonds are present in the final product (Khan et al., 2019).

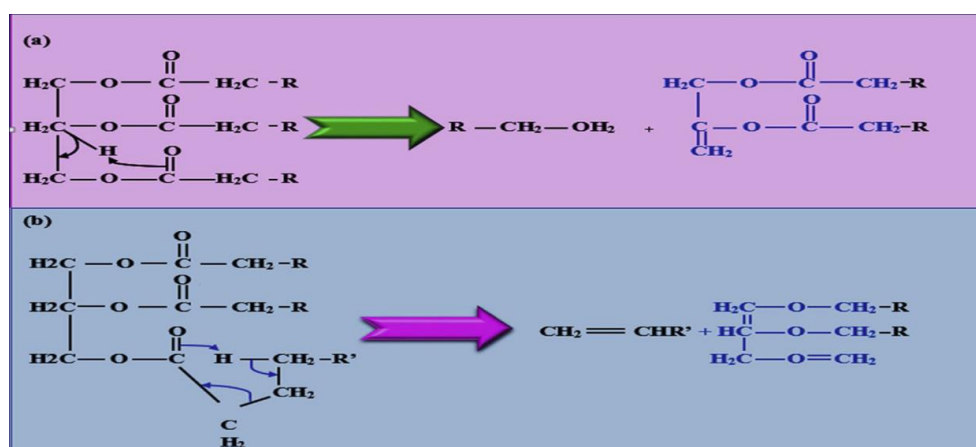


Figure 2.8 Dominant pathways in the thermal cracking of triglyceride determined by (a) β -elimination and (b) γ -hydrogen transfer (Khan, Lup et al. 2019).

2.6.2 Deoxygenation

Deoxygenation method is used to remove oxygen from a bio-based feed stock. The large amounts of oxygenated compound are present in the vegetable oil would hinder the application as fuel due to the challenges both in storage and usage in internal combustion engines. Various combinational reaction pathways of the deoxygenation of biomass can take place depending in the feedstock composition, catalyst choice, and reaction condition. Decarboxylation (DCO_2), decarbonylation (DCO) and Hydrodeoxygenation (HDO) are the main reaction route in deoxygenating biomass to bio-gasoline fuel (Rai and Da Silva, 2017). The process of deoxygenation of triglyceride can be simply generalized as **Figure 2.9**. The hydrodeoxygenation reaction results in the formation of hydrocarbons with chains of the same number of

carbons, along with water and propane. Decarboxylation and decarbonylation produces paraffin with one carbon less than that of the corresponding fatty acid and liberates CO₂ or CO (Mohammad *et al.*, 2013).

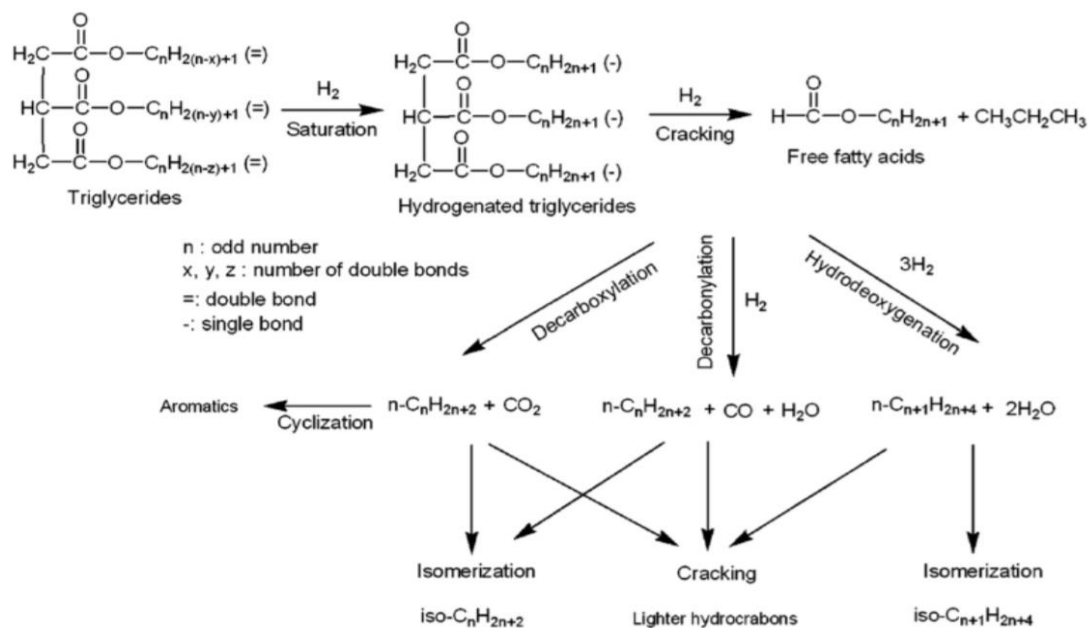
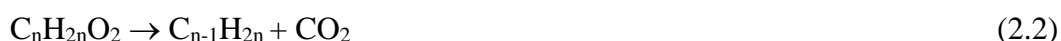


Figure 2.9 The possible deoxygenation pathways (Mohammad, Hari et al. 2013).

2.6.2.1 Decarboxylation (DCO₂)

Decarboxylation (DCO₂) is the reaction to remove carboxyl group in H₂ environment in which oxygen (O₂) is eliminated in the form of carbon dioxide (CO₂) from triglyceride carbon chain. The major products of DCO₂ reaction are C₁₅ and C₁₇ hydrocarbons which correspond to n-pentadecene and n-heptadecene respectively and leading to hydrogen generation during bond scission. DCO₂ reaction is responsible to form straight chain hydrocarbon (alkane) with one carbon lesser as shows in Eq.2.2 and **Figure 2.9** (Khan et al., 2019).



2.6.2.2 Decarbonylation (DCO)

Decarbonylation (DCO) reaction refers to the removal of carbonyl group in H₂ environment to produce alkanes with one carbon lesser than the original fatty acid and CO as a byproduct (Khan et al., 2019). DCO reaction pathways

using tristearin as a model compound of triglyceride to get n-pentadecane, CO and H₂O under H₂ pressure, as illustrated in Eq.2.3 and **Figure 2.10** . While complete reaction mechanism of both DCO₂ and DCO of tristearin into straight chain hydrocarbons (Santillan-Jimenez and Crocker, 2012).

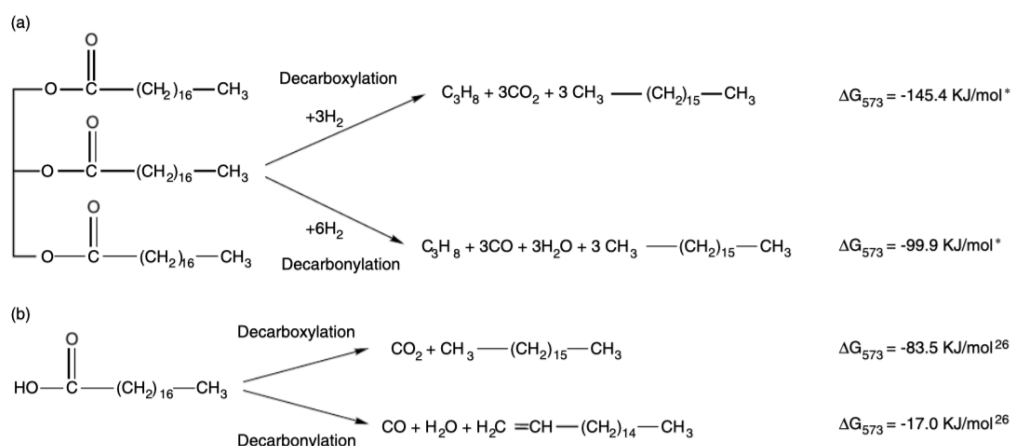


Figure 2.10 Decarboxylation and decarbonylation of (a) tristearin and (b) stearic acid (Pattanaik and Misra 2017).

2.6.2.3 Hydrodeoxygenation (HDO)

Hydrodeoxygenation is a process which incorporates the transformation of the unsaturated fatty acids in the vegetable oil into saturated fatty acids. During the process, oxygen removal from the fatty acids structure occurs in the form of the water at higher temperature and H₂ pressure as mentioned in Eq.2.4 and **Figure 2.11** . The primary objectives of HDO are to reduce the O/C ratio and at the same time to increase the H/C ratio. Hydrodeoxygenated vegetable oil possesses lower viscosity, zero oxygen content, superior atomization, and lubricity. It possesses very high cetane number and hence, suitable as a commercial replacement to diesel. During HDO process water is formed as the major by-product, which may reduce the catalyst activity. HDO of fatty acid results in high hydrocarbon yield even with a small amount of feed (Pattanaik and Misra, 2017).



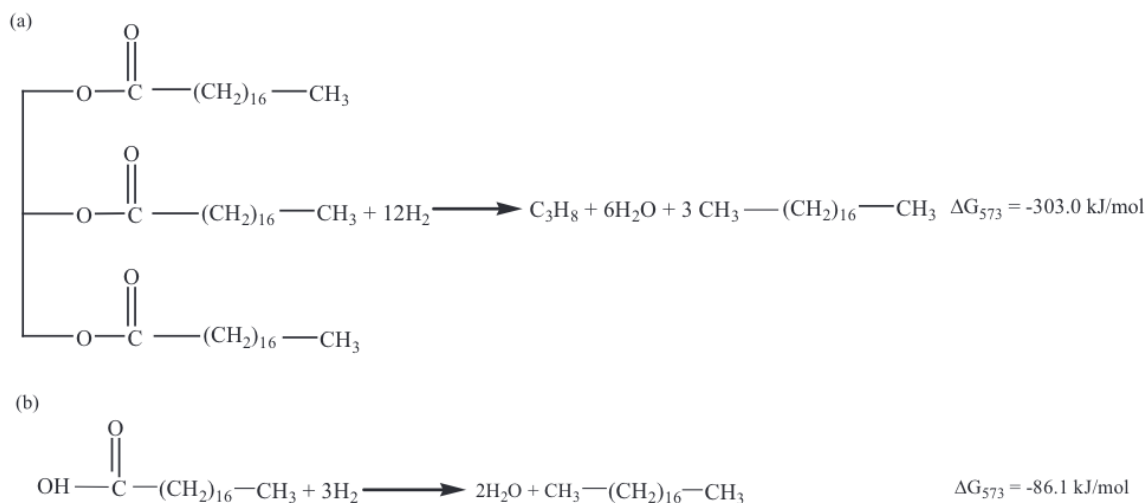


Figure 2.11 Hydrodeoxygenation reaction scheme for model compounds of triglycerides and fatty acids (a) tristearin and (b) stearic acid with thermodynamic data (Pattanaik and Misra 2017).

Silva *et al.* (2016) investigated deoxygenation catalyst by 5% of palladium on charcoal (Pd/C) reduce *in situ* using crude and previously macauba pulp and almond oils with different composition and acidity values to study the effect of the fatty composition and nature of the feedstock, reaction pressure, atmosphere, presence of stirring and use of Pd/C catalyst. The result indicated high selectivity, with a dominance of saturated linear hydrocarbons that correspond to green diesel followed by bio-jet fuel hydrocarbons. Oxygen removal was favored for free fatty acid with long carbon chains, for which DCO and/or DCO₂ predominates. The highest content of hydrocarbon (85% w/w) was obtained in the reaction of hydrolyzed macauba almond oil at 10 bars of H₂ pressure, 300°C, 5 h of reaction and stirring at 700 rpm.

2.6.3 Cracking and Isomerization Reactions

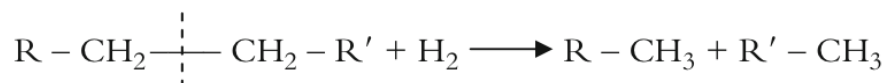
Cracking and isomerization reaction are used to improve the hydrodeoxygenation (HDO) process. HDO generally produce paraffinic hydrocarbons with high cetane number, but these paraffinic oils may have compatible issue with jet fuels due to their poor cold flow properties. Therefore, it is essential to improve their physiochemical properties by hydrocracking and isomerization reaction. Hydrocracking reaction is the process that converted paraffins to C₉-C₁₅ hydrocarbons chains which are suitable for jet fuel application. Hydroisomerization reaction is the

process that alkanes retain the high cetane number and improve the cold flow properties (Khan *et al.*, 2019).

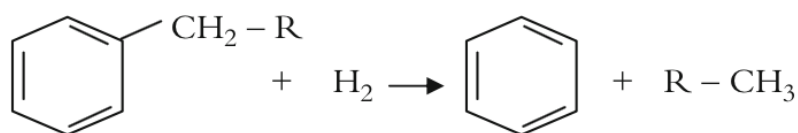
2.6.3.1 Hydrocracking

Hydrocracking is a catalytic hydrogenation process in which high molecular weight feedstocks are converted and hydrogenated to lower molecular weight products. The catalyst used in hydrocracking is bifunctional catalyst. It is composed of a metallic part, which promotes hydrogenation and an acid part, which promotes cracking. Cracking will break bonds, and the resulting unsaturated product are consequently hydrogenated into stable compounds. In the petroleum refineries used hydrocracking for the conversion of the middle and heavy distillates and residuals that have high-boiling range into more valuable lower boiling products such as gasoline, kerosene, jet fuel and diesel oil. **Figure 2.12** presents a hydrocracking reaction (Fahim *et al.*, 2009).

1. Alkane hydrocracking



2. Hydrodealkylation



3. Ring opening

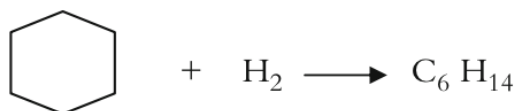


Figure 2.12 The schematic of hydrocracking reaction (Fahim, Al-Sahhaf *et al.* 2009).

Hydrocracking of *n*-paraffins over a bifunctional catalyst goes through the following steps:

1. Adsorption of *n*-paraffins on metal sites.
2. Dehydrogenation with formation of *n*-olefins.
3. Desorption from metal sites and diffusion to acid sites.

4. Skeletal isomerization and/or cracking of olefins on the acid sites through carbenium ion intermediates.
5. Desorption of formed olefins from acid sites and diffusion to metal site.
6. Hydrogenation of these olefins (n- and iso-) in the metal sites.
7. Desorption of resulting paraffins (Scherzer and Gruia, 1996).

2.6.3.2 Hydroisomerization

Hydroisomerization is an industrial process employed by petroleum refineries for the transformation of linear paraffins into their corresponding isomers at usually high hydrogen pressure at least 20 bars, although recent studies indicated that the reaction can be achieved at 1 atm. The process normally proceeds over a supported catalyst with bifunctionality. Normal paraffin to be converted undergo initial dehydrogenation over the metal sites to produce a corresponding n-alkane with the same number of the carbon chain. The interaction of the latter with Brønsted acid sites generates carbenium ion, which undergo subsequent isomerization into iso-carbenium ion and consequently desorbs as iso-alkane. The final stage of the reaction involved the hydrogenation of the latter over metallic sites to produce the desired branch paraffin as shown in **Figure 2.13** (Galadima and Muraza, 2015).

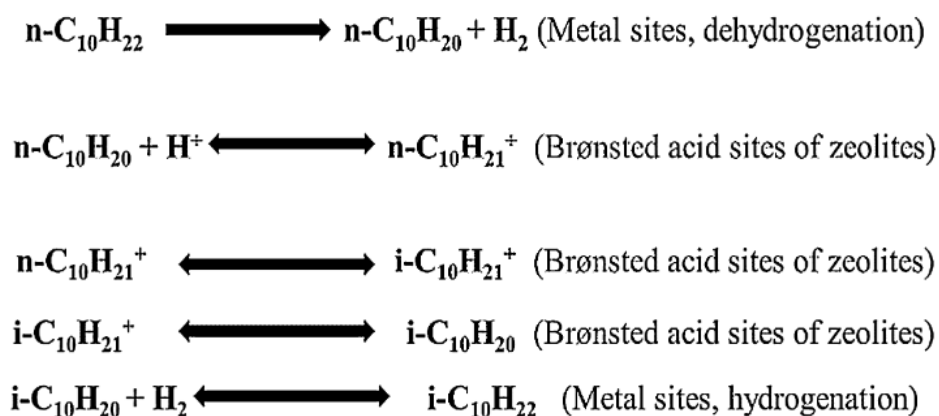


Figure 2.13 Mechanism of n-paraffins/n-alkanes hydroisomerization over bifunctional catalysts using n-decane as a model compound (Galadima. and Muraza., 2015).

2.7 The Catalyst for Biofuel Production

To produce hydrocarbons with biofuel property, the deoxygenation process optimization and catalysts have been intensively studied for upgrading of oil-based feedstocks, including vegetable oil, fats, and fatty acid. Catalyst pore structure, pore volume, surface area and acidity are some of the important properties which have significant effects on cracking properties. The catalyst that is used for the hydrocracking of vegetable oil are mainly sulphided forms of silica- and alumina-supported NiMo, CoMo and NiW. Therefore, the use of these catalysts needs the addition of sulphur containing compounds such as H₂S or dimethyl disulphide to maintain the activity of the catalysts.

Veriansyah *et al.* (2012) studied the effect of various catalysts on the hydroprocessing of soybean oil to produce a paraffin-rich mixture of hydrocarbon using a batch reactor system to compare the hydroprocessing conversion. The result found that at a catalyst/oil weight ratio 0.044 sulfide NiMo/ γ -Al₂O₃ (92.9%) has the highest conversion, follow by 4.29 wt% Pd/ γ -Al₂O₃ (91.9%), sulfide CoMo/ γ -Al₂O₃ (78.9%), 57.6 wt%. Ni/SiO₂-Al₂O₃ (60.8%), 4.95% wt% Pt/ γ -Al₂O₃ and 3.06 wt%. Ru/ γ -Al₂O₃ (39.7%), respectively. The straight chain α -alkane content was more than 80 wt% with the Pd or Ni catalyst.

Srifa *et al.* (2014) investigated the palm oil deoxygenation in a trickle bed reactor with the aim at optimizing the operation condition including temperature, H₂ pressure, LHSV, and H₂/oil ratio. It turned out that the temperature played a crucial role on reaction pathways (decarbonylation, decarboxylation, hydrodeoxygenation, hydrocracking, hydroisomerization) over NiMoS₂/ γ -Al₂O₃, meanwhile the increase in the H₂ pressure promoted the hydrodeoxygenation. The reaction conditions for high product yield (over 95%) were at temperature, 300°C, 3-5 MPa, LHSV 1-2 h⁻¹ and H₂/oil ratio is 750-1000 N(cm³/cm³).

However, the use of this sulphiding agents causes sulphur residues in the final products, H₂S emissions and corrosive problems. The combustion of this product may produce SO_x ozone and other greenhouse gases, which are responsible for pollution and global warming (Shahinuzzaman *et al.*, 2017). Through the cost of

noble metal was high. It became essential to develop non-sulfide transition metal catalyst for the hydrodeoxygenation of fatty acid to produce non-sulfur hydrocarbon fuel (Pattanaik and Misra, 2017).

Snare *et al.*, (2006) studied deoxygenation of fatty acid to produce biodiesel by using metal supported catalyst. The metal studied were Ni, Mo, Pd, Pt, Ir, Ru, Rh, and Os on Al₂O₃, Cr₂O₃, MgO and SiO₂ as well as on activated carbon. The deoxygenation reaction is carried out in a semi-batch reactor under constant temperature and pressure, 300 °C and 6 bar, respectively. The catalytic deoxygenation of stearic acid over heterogeneous catalysts was successfully achieved to the heptane with high activity and selectivity. The outcome of comparison with different metal on the equivalent supports by normalizing the results with metal content depicted that the beneficial effect of a metal in the deoxygenation reaction is in the descending order Pd > Pt > Ni > Rh > Ir > Ru and Os.

2.7.1 Zeolite as a Catalyst for Bio-jet Fuel Production

Zeolite is a complex molecule containing different ratio of silica to alumina and have three-dimensional tetrahedra. Tetrahedra have linked each other by shared oxygen atom to give cavities, which are connected by ring or pore openings, with defined size and shape shown in **Figure 2.14** (Ramsay and Kallus, 2000). Porous structure exhibits a potent catalytic activity to produce biofuel by the simultaneous cracking and dehydration reactions. Zeolite catalysts have versatile catalyst abilities because of its chemical composition, pore size distribution and ion-exchange ability. Furthermore, zeolite have both acidic and basic characteristics. It can be widely used as an industrial heterogeneous catalyst because they are inexpensive and environmentally friendly. Zeolites possess the general formula, $M_{x/n}[(AlO_2)_x(SiO_2)_y] \cdot zH_2O$, where M is an extra-framework cation that balances the anionic charge of the framework. Generally, zeolites are classified as one of three types depend on their pore volume. There is small-pore zeolite that have diameter between 2.8 to 4.0 Å containing with 6-8 member rings, medium-pore zeolite has that have diameter between 5.0 to 6.0 Å containing with 10 member rings and large-pore zeolite that have diameter more than 7.0 Å containing with 12 member rings. The most common zeolite catalysts for the catalyst cracking of vegetable oil are ZSM-5, HY, ZSM-12, SAPO-

11, SBA-15, Meso-Y, MCM-41, Ultrastable Zeolite (USYZ) and beta zeolite (Shahinuzzaman *et al.*, 2017).

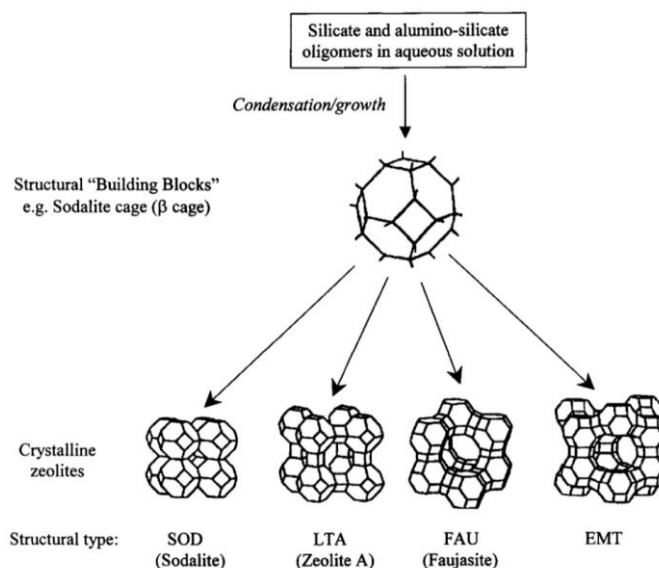


Figure 2.14 Oligomeric silicate and aluminosilicate species can form structural units or building blocks, which subsequently organize to give different zeolite structures (Ramsay and Kallus 2000).

Cheng *et al.* (2014) investigating bio jet fuel converted by soybean oil using two zeolites of HY and HZSM-5 supporting Ni and Mo. Resulting show the Zeolite HY was higher jet range selectivity (40.3%) and lower jet range aromatic hydrocarbon selectivity (23.8%) than zeolite HZSM-5 (13.8 and 58.9%). Moreover, a high yield of jet fuel (48.2%) was obtained at 1 MPa low H₂ pressure over Ni (8 wt.%)- Mo (12 wt.%) /HY catalyst.

Ju *et al.* (2016) studied the high yield jet fuel production process by integration of rational feed stock reaction and selective hydrocarbon isomerization using Pt/USYZ, Pt/HZSM-12 and Pt/HZSM-22 catalyst with the condition of 3 MPa H₂ pressure and temperature at 200-340 °C. The result show that Pt/HZSM-12 catalyst was an effective catalyst for conversion of n-C₁₅ paraffin into multi-branch isomers and mono-branch isomers which satisfied the jet fuel specification.

2.7.2 Active Metal and Promoter

Most industrial hydroisomerization catalysts are based on zeolites, which provide the acid function. As the hydrogenation and dehydrogenation, various species of metals have been tested including Pd, Pt, Ni, Rh, Ir, Ru, and Os. Mostly associated with mordenite or CaY. Bifunctional catalysts, with both hydrogenation and dehydrogenation and isomerization have shown high efficiency in alkane hydroisomerization. Noble metal-zeolite catalysts especially Pd or Pt loaded Y, mordenite and beta leads a high activity and selectivity for hydroisomerization of n-alkane (De Lucas *et al.*, 2006).

Nickle is very active metal in hydrogenation catalysis. It is also a cheap element thus allowing its use as a bulk metal (e.g., as Raney nickle) as well as in the form of highly loaded supported catalysts. This also gives rise to some sulfur resistance, just because mush sulfur is needed to fully poison highly loaded catalysts. On the other hand, the carcinogenic toxicity of nickel compounds is a big concern in the preparation and disposal of catalysts. Many investigators have recognized that nickel oxide when supported on kieselguhr gives much more active catalysts than an unsupported one, although the reduction temperature required for the supported oxide (350-500 °C).

Peng *et al.* (2012) studied the selective deoxygenation of stearic acid and Microalgae oil over Ni catalysts support on different two types of catalysts (HZSM-5 and H-Beta) of varying Si/Al ratio using batch reactor. Full conversion of stearic acid was obtained over 10% Ni/HZSM-5 (Si/Al = 45) catalysts, but severe cracking of the produced alkanes selectivity 43% in range C₁₇ and C₁₈ was observed own to its high acidity.

Lai *et al.* (2016) studied formation of Pd or Pt overlayer on Ni base metal would cause a negative shift of the d-band center of surface Pd or Pt, resulting in reduced binding strength for adsorbed species. Silica alumina supported Ni@Pd and Ni@Pt over layer catalysts were synthesis via directed desorption technique and tested for hydrodeoxygenation of guaiacol at atmospheric pressure. Guaiacol hydrodeoxygenation results show at the low temperature, Pd and Pt actives sites of overlayer catalysts showed significantly enhanced deoxygenation activity compared with the only Pd and Pt catalysts.



378235724

CU IThesis 6271009063 thesis / revv: 13092564 11:18:12 / seq: 50

Zhang and Zhao (2016) studied effect Pd-Ni/HZSM-5 catalyst for tandem process involving the deoxygenation of the terpene limonene and the hydrodeoxygenation of stearic acid. The process involves the generation of p-cymene from terpene with concomitant formation of H₂ as a product. Directly incorporating Pd and Ni onto the HZSM-5 scaffold forms the Pd-Ni/HZSM-5 bimetallic catalyst, which demonstrates a remarkable improvement in stearic acid conversion to C₁₇ and C₁₈ alkane products. In this catalyst system, Pd was shown to be the active site for limonene dehydroaromatization, while Ni catalyzes the separate stearic acid hydrodeoxygenation. The acidity of HZSM-5 (modified by the Si/ Al ratios) influences the performance of the Pd-Ni bimetallic catalyst, and the proper pore size of HZSM-5 prevents side-reactions from limonene condensation.

2.7.3 Chemical Liquid Deposition (CLD)

Chemical liquid deposition (CLD) is a common surface modification technology used for external surface modification of catalysts. CLD could change the pore-opening size and reduced amount of acid sites on the surface of catalyst. Moreover, CLD method has many advantages, such as simple equipment, low cost and easy to operation. Thus, it is used widely to modified catalysts in the field of petrochemical engineering. In CLD process, modifier with molecular diameter which is greater than pore diameter of catalyst deposits on the external surface to modify acid sites of the catalyst to achieve high selectivity of the products and preferable resistance to coking properties. On the other hand, CLD method used for reducing external acid sites is the selective removal of aluminum in the zeolite framework (Zhang *et al.*, 2017).

Hou *et al.* (2016) studied catalytic cracking of *n*-pentane over CLD-modified HZSM-5 zeolites. The results found that the CLD-modified catalysts gave a maximum 46% promotion of catalytic activity using the catalytic cracking *n*-pentane as a model reaction at 500 °C, attributed to the enhanced sorption process caused by porous overlayer. In addition, TiO₂-CLD modified zeolites exhibited a better catalytic cracking performance compared with SiO₂ that was probably due to the extra Lewis acid site generated by TiO₂.

Zhang, Wang, *et al.* (2018) studied (CLD)-modified Fe-ZSM-5 for enhanced activity and resistance to C₃H₆ poisoning in selective catalytic reduction

with NH_3 . They use chemical liquid deposition technique to dope a shell layer of SiO_2 . The results show that it acts as a protective layer against C_3H_6 while providing abundant Lewis's acid sites. Which compensate for the relatively less Fe-active sites and contribute to higher overall selective catalytic reduction (SCR) activities and better resistance to C_3H_6 poisoning.

Feng *et al.* (2020) studied Ni/ZSM-5 nanosheet catalysts with different Si/Al ratios (100, 200 and 300) were modified by chemical liquid deposition (CLD) of tetraethyl orthosilicate (TEOS) to tailor acid spatial distribution. Their catalytic performance was evaluated with the hydroconversion of oleic acid to aviation-fuel-range-alkanes (AFRAs) at different reaction temperature and H_2 pressure. The modified catalysts showed similar structure, Ni dispersion and internal acid concentration but lower concentration. The deoxygenation and cracking reactions were also more sensitive to H_2 pressure compared to the isomerization reaction. NS200(1) had a high selectivity of 51.4% as well as high iso/n-alkanes ratio of 1.7 were achieved at 250 °C and 10 bars.



378235724

CHAPTER 3

METHODOLOGY

3.1 Materials and Equipment

Material

Feedstock

- Palm fatty acid distillate (PFAD: obtained from Global Green Chemicals Public Co., Ltd)

Chemical

- Nickel (II) nitrate hexahydrate purum p.a., crystallized, $(\text{Ni}(\text{NO}_3)_2 \cdot 6\text{H}_2\text{O})$, 97.0% purity, Sigma Aldrich)
- Palladium (II) chloride Reagent Plus (PdCl_2 , 99% purity, Sigma Aldrich)
- The commercial ZSM-5 (with Si/Al ratio = 23, 50 and 280) was supplied from Zeolyst, USA
- Hydrochloric acid (HCl 37 wt%, EMSURE)
- Cyclohexane (C_6H_{12} , 99.5% purity, LOBA)
- Tetraethyl orthosilicate (TEOS, 99.0% purity, Sigma Aldrich)
- Dichloromethane (CH_2Cl_2)
- Pyridine ($\text{C}_5\text{H}_5\text{N}$, 98% purity, Carlo Erba)
- N,O-bis (trimethylsilyl)-trifluoro acetamide (BSTFA, $\text{C}_8\text{H}_{18}\text{F}_3\text{NOSi}_2$, 99% purity, Sigma Aldrich)
- Acetone (CH_3COCH_3 , 98% purity, Labscan)
- Methanol (CH_3OH , 99.9% purity, Labscan)
- Hexane (C_6H_{14} , 99.9% purity, Labscan)
- Deionized water

Gases

- Hydrogen (99.99% purity, BIG)
- Nitrogen (99.99% purity, Linde)
- Helium (99.99% purity, Linde)

- Air zero (99.99% purity, Linde)

Equipment

- High pressure packed-bed continuous flow reactor system consisting of
 - Mass flow controller (Brook's instrument 5850E)
 - Teledyne ISCO syringe pumps 100D
 - Back pressure regulator (SOEMENS)
 - $\frac{3}{4}$ " O.D. 16-inch-long stainless-steel reactor
- Three-zone tubular furnace with a temperature controller (Cabolite)
- Gas chromatograph (Agilent GC 7890 equipped with injector, DB-5HT column and FID)
- Gas chromatograph (Hewlett Packard 5890 series II, HP-PLOT/Al₂O₃ column)
- Chamber furnace (Cabolite)
- X-ray diffractometer (XRD, Rigaku/Smartlab)
- X-ray fluorescence spectrometry (XRF)
- X-ray photoelectron spectroscopy (XPS)
- Transmission electron microscopy (TEM)
- Surface area analyzer (Brunauer-Emmett-Teller)
- Hot & stirrer plate (Cole Parmer)
- Oven

3.2 Experimental Procedures

3.2.1 Catalyst Preparation

3.2.1.1 *Chemical Liquid Deposition (CLD)*

The external surface of ZSM-5 zeolites was modified with SiO₂ phase by CLD method. Firstly, tetraethyl orthosilicate (TEOS) was added into the cyclohexane with intense stir. Then commercial zeolite after calcined at 550 °C for 5 h with a heating rate of 10 °C/min was added into the homogeneous solution and stirring for 1 h. The resulted products were repeatedly washed with cyclohexane and dried at 120 °C for 2 h. Then, the sample was calcined at 550 °C for 5 h with heating



378235724

CU Theses 6271009063 thesis / rev: 13092564 11:18:12 / seq: 50

rate 10 °C/min. The ZSM-5 with Si/Al ratios of 50 and 280 were carried out once while ZSM-5 with Si/Al ratio of 23 was carried out twice in CLD process.

3.2.2 Metal Loading on Zeolite Support

The metals were loading in zeolite supports by incipient wetness impregnation method. PdCl₂ was firstly dissolved in HCl solution (conc. 37%) at 80 °C to afford H₂PdCl₄ solution. For Ni metal loading, Ni (NO₃)₂ • 6H₂O was dissolved in water at a volume of water equal to the pore volume of ZSM-5 zeolites. The Ni and Pd precursors were mixed and slowly dropped onto the zeolite support. After that the mixture was gradually dried in oven at 120 °C to remove excess water for overnight. The dried catalyst was calcined at 500 °C for 6 h with heating rated of 10 °C/min.

3.3 Catalyst Characterization

3.3.1 X-ray Diffraction (XRD)

X-ray diffraction was used to determine the information about crystalline phase of synthesized catalyst by a Rigaku X-ray diffractometer, RINT-2200 with Cu tube generating CuK α radiation (1.5406 Å) and operating condition of 40 kV. The sample was measured in the 2 θ range of 5-90° with a scanning of 5°/min and step rate 0.02° s⁻¹.

3.3.2 Brunauer-Emmett-Teller (BET)

The surface areas of the fresh and spent catalysts were measured by BET surface are analyzer (Quantachrom/Autosorb 1-MP instrument). The sample was first outgassed to remove the humidity and volatile adsorbents adsorbed on surface under vacuum at 250 °C for 10 h prior to the analysis. Then, N₂ was purged to adsorb on surface, measuring the quantity of gas adsorbed onto or desorbed from their solid surface at some equilibrium vapor pressure by static volumetric method. The solid sample was maintained at a temperature of the sample cell until the equilibrium is established. This volume-pressure data will be used to calculate the BET surface area.



3.3.3 Transmission Electron Microscopy (TEM)

The morphology of prepared catalyst was observed by a transmission electron microscopy (JEM-1400). The sample was prepared by dispersing on the carbon coat film coating TEM grid then it was suspended in isopropanol solvent. The sample was inserted into the TEM instrument. Then, the beam of electrons (120 kV) from the electron gun was transmitted through a sample to form a TEM image.

3.3.4 X-ray Fluorescence Spectrometry (XRF)

X-ray fluorescence spectrometer (WDXRF S8-tiger) was used to determine elemental composition. For sample preparation, the sample was ground into a fine powder to minimize undesired particle size effects and compressed using a hydraulic press to form a pallet. After that, the sample holder was inserted in the XRF instrument. For the analysis, an X-ray beam with enough energy interacted with the atom by replacing electron from inner shell. Atom became unstable from missing inner electron than an outer electron replaced the missing inner electron. The replacement occurred the different energy between the X-ray beam from analyzer and the binding energy that held electrons in their proper orbits. The measurement of this energy is the basis of XRF analysis. When X-ray energy causes electrons to transfer in and out of electron orbitals, XRF peaks with varying intensities are created and presented in the spectrum, a graphical representation of X-ray intensities peaks as a function of energy peaks. The peak energy identifies the element, and the peak height or intensity is generally indicative of its concentration.

3.3.5 X-ray Photoelectron Spectroscopy (XPS)

X-ray photoelectron spectroscopy (Kratos/AXIS ULTRA DLD) was used to determine the chemical element on the surface of the catalysts. For sample preparation, the sample was dried in the oven, then ground and placed on the carbon tape at the surface of sample bar. After that, the sample bar was inserted into the XPS instrument. The instrument vacuum exceeded 5×10^{-8} Torr during the experiments. The spectra were recorded in constant analyzer energy mode at a pass energy of 140 eV for wide scan mode and 40 eV for narrow scan mode. All spectra were energy calibrated using the internal standard peak (C_{1s}) at the binding energy of 284.7 eV. The data was evaluated using the Vision Processing software, and the background subtraction applied to the high-resolution scans followed the method. Then, the

experimental curves were fit for giving deconvolution of XPS spectra. The position and intensity of the peaks in an energy spectrum provide the desired chemical state and quantitative information. The chemical environment of an atom alters the binding energy (BE) of a photoelectron which results in a change in the measured kinetic energy (KE). The BE is related to the measured photoelectron KE by the simple equation; $BE = hv - KE$ where hv is the photon (X-ray) energy. The chemical or bonding information of the element is derived from these chemical shifts.

3.4 Catalyst Activity Testing

Figure 3.1 and **Table 3.1** show the schematic of the reactor system and the description of flow diagram, respectively. The hydrodeoxygenation, hydrocracking, and isomerization reactions of palm fatty acid distillate (PFAD) were carried through a $\frac{3}{4}$ " O.D., continuous flow fixed bed reactor under high hydrogen pressure conditions. First, 4 mL of catalyst was reduced under flowing of H_2 for 3 h at the reaction temperature of 500 °C with heating rate of 10 °C/min. Then, the temperature and pressure of the reactor were set to the desired value in a flowing H_2 . The stream of PFAD was fed into the reactor by a Teledyne 1000D Isco syringe pump. Mass flow controller and back-pressure regulator were used for controlling the flow of carrier gas and the reaction pressure, respectively. During the process, the liquid product was trapped and collected in a condenser and gas product was analyzed online by using a Shimadzu GC-17A gas chromatograph equipped with a capillary HP-PLOT/ Al_2O_3 "S" deactivated column and FID detector. Amount of gas product was corrected by using a wet test gas meter (Ritter TG 05/2). Finally, the liquid product was derivatized by BSTFA and pyridine. After that, the sample was analyzed by another gas chromatograph, Agilent 7890 equipped with DB-5HT column and FID detector. Both gas product and liquid product were analyzed hourly.



3782235724

CD IThesis 6271009063 thesis / rev: 13092564 11:18:12 / seq: 50

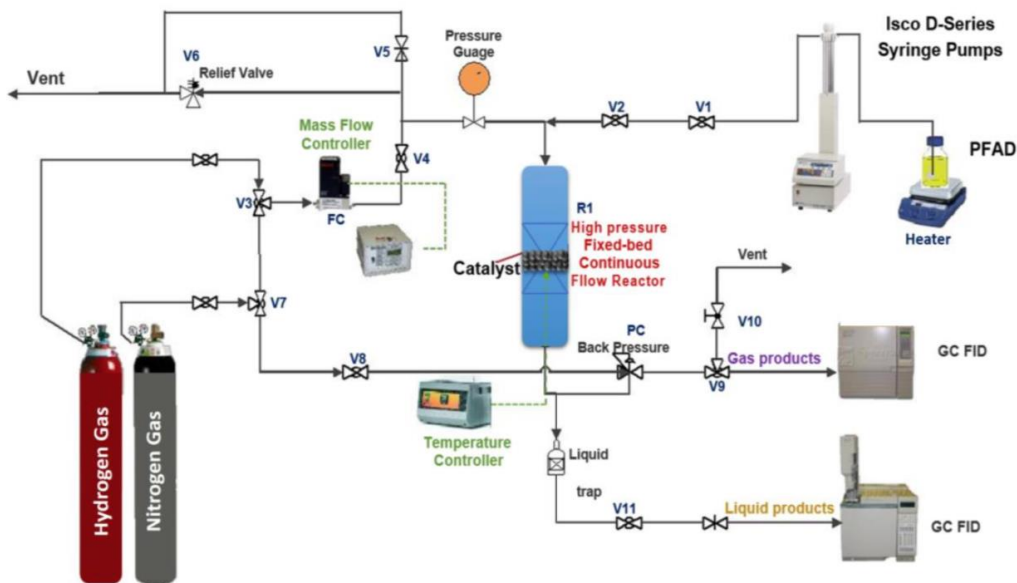


Figure 3.1 The schematic diagram of the reactor system.

Table 3.1 Description of system in flow diagram of the continuous flow fixed bed reactor

No.	Part	Description
1	V1	On-off valve for feedstock from ISCO syringe pumps.
2	V2	Checking valve for avoiding the backward flow of the feedstock.
3	V3	Three ways valve for switching between nitrogen gas and hydrogen gas flow.
4	V4	Checking valve for avoiding the backward flow of hydrogen or nitrogen gas.
5	V5	Needle valve for releasing gas from the system.
6	V6	Relief valve for releasing pressure overload in the system.
7	V7	Three ways valve for switching the direction of nitrogen gas flow.
8	V8	Needle valve for controlling pressure in back pressure regulator.
9	V9	Three ways valve for switching between vent gas and gas to GC lines.

Table 3.1 (Cont.) Description of system in flow diagram of the continuous flow fixed bed reactor

No.	Part	Description
10	V10	On-off valve for releasing pressure from back pressure regulator.
11	V11	Metering valve for gathering the liquid product from condenser.
12	R1	Continuous flow fixed bed reactor where hydroprocessing reaction take place. Flow controller to set flow rate for the desired H ₂ /feed molar ratio.
13	FC	Pressure gauge for indicating pressure in packed bed reactor.
14	PG	Back pressure regulator for controlling the pressure in reactor.
15	PC	

The hydroprocessing reaction of PFAD is performed at temperature, pressure, liquid hourly space velocity (LHSV), and H₂/feed ratio as shown in **Table 3.2**.

Table 3.2 The reaction conditions for hydroprocessing of palm fatty acid distillate in continuous flow fixed bed reactor

Parameter	Value
Reaction Temperature (°C)	325 - 375
Reaction Pressure (bar)	10 - 30
LHSV (h ⁻¹)	1.5 – 2.5
Volume of Catalyst (mL)	4
H ₂ /feed molar ratio	8
Carrier gas	H ₂

3.5 Product Analysis

3.5.1 Liquid Products Analysis

The liquid products were quantified by a gas chromatograph (Agilent 7890) equipped with FID detector. The liquid products from the hydrocracking of PFAD contain non-polar hydrocarbons. The non-polar hydrocarbons were determined by using DB-5 column (non-polar column).

The GC operating condition was summarized as follows:

Injector temperature: 50 °C



378235724

Detector temperature: 380 °C
 Carrier gas: He
 Column type: Capillary column
 (DB-5HT: diameter 0.32 mm length 30 m)

The following chromatographic program in **Table 3.3** was used for liquid product analysis:

Table 3.3 The chromatographic temperature program for liquid product analysis

Step	Temperature (°C)	Rate (°C/min)	Holding time (min)
1	50	-	5
2	169	10	10
3	380	20	10

For the quantitative calculations of liquid product, the areas of each peak analyzed hourly by a GC/FID (Agilent 7890) were converted to gram unit by Equation 3.1 because each peak of products detected by FID detector can be varied from area unit to gram unit directly.

$$\text{Weight of product } i \text{ (g)} = \frac{(\text{areas of product } i) \times (\text{grams of liquid product})}{\text{total areas of liquid product}} \quad (3.1)$$

The conversion and products selectivity of each product were calculated by Equation 3.2 and Equation 3.3.

$$\text{Conversion (\%)} = \frac{\text{moles of feed converted} \times 100}{\text{moles of feed input}} \quad (3.2)$$

$$\text{Selectivity to product } i \text{ (\%)} = \frac{\text{moles of product } i \times 100}{\text{moles of overall products}} \quad (3.3)$$

3.5.2 Gas Product Analysis

The composition of gas product was analyzed hourly by GC/FID (Hewlett Packard 5890 series II). The GC operating condition was summarized as follows:

Injection temperature: 150 °C
 Detector temperature: 250 °C
 Carrier gas: He

Column type: capillary HP-PLOT/Al₂O₃
 “S” deactivated column

The following chromatographic temperature program in **Table 3.4** was used for gas product analysis:

Table 3.4 The chromatographic temperature program for gas-phase product analysis

Step	Temperature (°C)	Rate (°C/min)	Holding time (min)
1	40	-	3
2	70	15	0
3	170	5	0
4	190	1	1

For the quantitative calculation of gas product, the areas of each peak analyzed hourly by GC/FID (Shimadzu GC-17A) were converted to gram unit by comparing with the area of methane from gas standard by mol% (equal to vol%), as shown in Equation 3.4.

$$\text{Weight of product i (g)} = \frac{(\text{areas of product i per 1 ml}) \times (\text{mol of methane per 1 ml}) \times (\text{overall gas product } \frac{\text{ml}}{\text{h}})}{(\text{mol of carbon atom}) \times (\text{reference area of methane per 1ml}) \times (\text{molecular weight } \frac{\text{g}}{\text{mol}})} \quad (3.4)$$

The calculation of conversion, selectivity and yield of product are defined as shown in Equations 3.5, 3.6 and 3.7, respectively.

$$\text{Conversion (\%)} = \frac{(\text{weight of feed input} - \text{weight of feed remaining}) \times 100}{\text{weight of feed input}} \quad (3.5)$$

$$\text{Selectivity of product i (\%)} = \frac{\text{weight of product i} \times 100}{\text{weight of total products}} \quad (3.6)$$

$$\text{Yield of product i (\%)} = (\text{conversion}) \times (\text{selectivity of product i}) \quad (3.7)$$

CHAPTER 4

RESULTS AND DISCUSSION

In this study, bimetallic NiPd supported on ZSM-5 with various Si/Al ratios (23, 50 and 280) and TEOS-modified ZSM-5 catalysts were prepared and characterized by X-ray diffractometer (XRD), Brunauer-Emmett-Teller (BET) surface area analyzer, X-ray fluorescence spectrometry (XRF), X-ray photoelectron spectroscopy (XPS) and transmission electron microscopy (TEM). The catalysts were investigated for their catalytic activity in converting PFAD to bio-jet fuel. Moreover, the optimum operating condition (i.e., temperature and pressure) for production of bio-jet fuel was also studied.

4.1 Characterization of Catalysts

4.1.1 X-ray Diffraction (XRD)

XRD patterns of the prepared catalysts i.e., ZSM-5, NiPd/ZSM-5 (23), TEOS-NiPd/ZSM-5 (23), TEOS(2)-NiPd/ZSM-5 (23) NiPd/ZSM-5 (50), TEOS-NiPd/ZSM-5 (50), NiPd/ZSM-5 (280), and TEOS-NiPd/ZSM-5 (280) catalysts are shown **Figure 4.1**. Firstly, the parent ZSM-5 had characteristic peaks at $2\theta = 8.3^\circ$, 9.2° , 23.5° and 24.3° corresponding to the planes (1,0,1), (2,0,0), (5,0,1) and (3,0,3), respectively. which were assigned to the MFI framework (Basir *et al.*, 2021). The XRD pattern of the TEOS-modified catalysts had a similar diffraction pattern as ZSM-5, which demonstrated that TEOS modification did not change the MFI framework of ZSM-5. However, the intensity of TEOS-modified catalysts slightly decreased as compared to the unmodified catalyst due to the presence of the amorphous SiO₂ layer (Feng *et al.*, 2020). Moreover, nickel oxide (NiO) exhibited obvious peaks at 37.07° (1,1,1), 43.09° (2,0,0) and 62.62° (2,2,0) (Srivastava and Srivastava, 2010), but palladium oxide (PdO) was not observed due to the low Pd loading.



378235724

CD IThesis 6271009063 thesis / rev: 13092564 11:18:12 / seq: 50

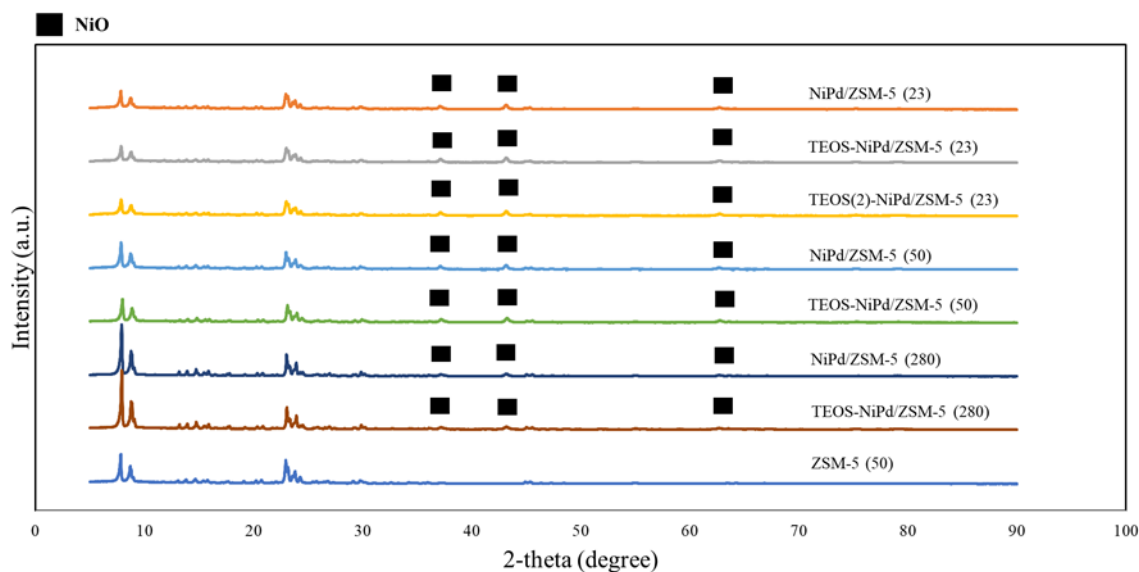


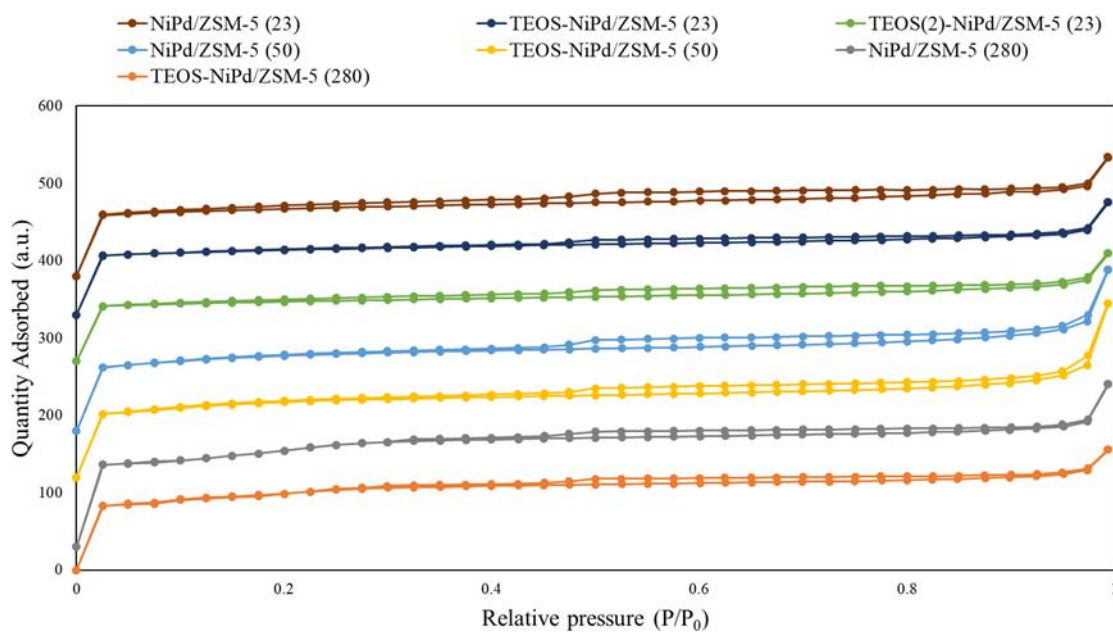
Figure 4.1 XRD patterns of the prepared catalysts.

4.1.2 Brunauer-Emmett-Teller (BET)

N_2 adsorption and desorption isotherms were used to characterize the pore properties of TEOS-modified and unmodified NiPd/ZSM-5 with various Si/Al ratios (23, 50 and 280). As shown in **Figure 4.2**, at low relative pressure from 0.0 to 0.2, all the prepared catalysts showed a point, indicating the microporous structure. At a high relative pressure from 0.5 to 0.9, the type IV isotherm with hysteresis loop in all catalysts indicated the existence of the mesoporous structure (Feng *et al.*, 2020). This result shows that both microporous and mesoporous structure appeared in the prepared catalysts. The physical characteristics of the prepared catalysts are summarized in **Table 4.1**. The total surface area was calculated by the Brunauer-Emmett-Teller (BET) equation. External surface area, micropore surface area and micropore volume were obtained by V-t method, and total pore volume was obtained by Barrett-Jayner-Halenda (BJH). The results showed that the TEOS-modified catalysts had a slightly decrease micropore surface area, indicating that the TEOS modification had no effect on the micropore surface properties. However, the obvious decrease was observed in the external surface area of TEOS-modified catalysts, indicating that TEOS modification mainly affected on the external surface of the ZSM-5 zeolites because the TEOS molecule is larger than the pore size of ZSM-5 (0.54 x 0.56 nm) (Zhao *et al.*, 2016).

Table 4.1 Physical characteristics of the prepared catalysts analyzed by BET

Catalysts	S_{BET} (m^2/g)	S_{ext} (m^2/g)	S_{mic} (m^2/g)	V_{total} (cm^3/g)	V_{mic} (cm^3/g)	V_{mes} (cm^3/g)
NiPd/ZSM-5 (23)	263	83	180	0.238	0.098	0.140
TEOS-NiPd/ZSM-5 (23)	252	73	179	0.226	0.098	0.128
TEOS (2)-NiPd/ZSM-5 (23)	230	59	172	0.216	0.093	0.123
NiPd/ZSM-5 (50)	328	175	163	0.349	0.088	0.261
TEOS-NiPd/ZSM-5 (50)	299	138	159	0.323	0.086	0.237
NiPd/ZSM-5 (280)	349	241	107	0.252	0.050	0.202
TEOS-NiPd/ZSM-5 (280)	319	217	103	0.226	0.047	0.179

**Figure 4.2** N_2 adsorption and desorption isotherms of the prepared catalysts.

4.1.3 Chemical Composition

X-ray fluorescence (XRF) technique was used to study the chemical composition of the prepared catalysts. As shown in **Table 4.2**, the Ni contents in the prepared NiPd/ZSM-5 (23), TEOS-NiPd/ZSM-5 (23), TEOS (2)-NiPd/ZSM-5 (23) NiPd/ZSM-5 (50), TEOS-NiPd/ZSM-5 (50), NiPd/ZSM-5 (280), and TEOS-NiPd/ZSM-5 (280) catalysts were 9.58%, 9.03%, 8.89%, 8.61%, 8.84%, 6.41% and 6.13%, respectively. The Pd contents in the prepared NiPd/ZSM-5 (23), TEOS-NiPd/ZSM-5 (23), TEOS (2)-NiPd/ZSM-5 (23) NiPd/ZSM-5 (50), TEOS-NiPd/ZSM-5 (50), NiPd/ZSM-5 (280), and TEOS-NiPd/ZSM-5 (280) catalysts were 0.695%, 0.761%, 0.676%, 0.621%, 0.729%, 0.542% and 0.575%, respectively. The Ni and Pd contents were unexpectedly lower than the design amount, especially the ones with high Si/Al ratios. This could be due to the loss during catalyst preparation over different affinity supports.

Moreover, The Si/Al ratios in the bulk and external surface of the catalysts were analyzed by X-ray fluorescence spectrometry (XRF) and X-ray photoelectron spectroscopy (XPS), respectively. The results are shown in **Table 4.3**. The Si/Al ratio at the external surface of NiPd/ZSM-5 (23), TEOS-NiPd/ZSM-5 (23), TEOS (2)-NiPd/ZSM-5 (23) NiPd/ZSM-5 (50), TEOS-NiPd/ZSM-5 (50), NiPd/ZSM-5 (280), and TEOS-NiPd/ZSM-5 (280) catalysts were 14.98, 18.49, 22.13, 32.97, 56.51, 113.18, and 134.46, respectively. Moreover, the Si/Al ratio from XRF of NiPd/ZSM-5 (23), TEOS-NiPd/ZSM-5 (23), TEOS (2)-NiPd/ZSM-5 (23) NiPd/ZSM-5 (50), TEOS-NiPd/ZSM-5 (50), NiPd/ZSM-5 (280), and TEOS-NiPd/ZSM-5 (280) catalysts were 12.41, 12.43, 12.86, 29.63, 30.85, 102.62, and 103.66, respectively. Therefore, the Si/Al ratio from XRF of the TEOS-modified catalysts was slightly increased from the unmodified catalyst due to the presence of Si. However, the Si/Al ratio on the external surface of the TEOS-modified catalysts had higher than the unmodified catalyst, indicating that the Si was mainly observed on the external surface corresponded to the BET results (Feng *et al.*, 2020).



378235724

CD IThesis 6271009063 thesis / rev: 13092564 11:18:12 / seq: 50

Table 4.2 Chemical composition of the prepared catalysts analyzed by XRF

Catalysts	Ni (wt.%)		Pd (wt.%)	
	Theory	XRF	Theory	XRF
NiPd/ZSM-5 (23)	10	9.58	1	0.70
TEOS-NiPd/ZSM-5 (23)	10	9.03	1	0.76
TEOS (2)-NiPd/ZSM-5 (23)	10	8.89	1	0.68
NiPd/ZSM-5 (50)	10	8.61	1	0.62
TEOS-NiPd/ZSM-5 (50)	10	8.84	1	0.73
NiPd/ZSM-5 (280)	10	6.41	1	0.54
TEOS-NiPd/ZSM-5 (280)	10	6.13	1	0.57

Table 4.3 Si/Al ratio of the prepared catalysts analyzed XPS and XRF

Catalysts	Si/Al ratio from XPS			Si/Al ratio from XRF		
	Si atomic %	Al atomic %	Si/Al atomic ratio	Si atomic %	Al atomic %	Si/Al atomic ratio
NiPd/ZSM-5 (23)	8.09	0.54	14.98	36.5	2.94	12.41
TEOS-NiPd/ ZSM-5 (23)	9.43	0.51	18.49	36.3	2.92	12.43
TEOS (2)-NiPd/ZSM-5 (23)	12.17	0.55	22.13	36.4	2.83	12.86
NiPd/ZSM-5 (50)	11.54	0.35	32.97	40.0	1.35	29.63
TEOS-NiPd/ZSM-5 (50)	18.65	0.33	56.51	39.8	1.29	30.85
NiPd/ZSM-5 (280)	18.11	0.16	113.18	43.1	0.42	102.62
TEOS-NiPd/ZSM-5 (280)	20.17	0.15	134.46	42.5	0.41	103.66

4.1.4 Transmission Electron Microscopy (TEM)

TEM images of the parent ZSM-5 (5), NiPd/ZSM-5 (50), and TEOS-NiPd/ZSM-5 (50) are shown in **Figure 4.3**. In **Figure 4.3** (a), the parent ZSM-5 (50) had a hexagonal plate shape with a smooth surface and crystal size approximately around 100 nm (Silva et al., 2019). **Figure 4.3** (b) and (c) show the NiPd/ZSM-5 (50) and TEOS-NiPd/ZSM-5 (50) which were the sample of unmodified catalyst and

TEOS-modified catalyst. The amorphous of SiO₂ layer was not clearly observed after modified ZSM-5 (50) by TEOS in the TEM image of TEOS-NiPd/ZSM-5 (50) due to the small SiO₂ layer less than 5 nm (Zhang, Shi, et al., 2016). Moreover, TEOS-NiPd/ZSM-5 (50) showed the similar hexagonal plate shape and crystal size as NiPd/ZSM-5 (50), indicating the TEOS-modified catalyst had the same morphological structure as the unmodified catalyst. In addition, the dark spots can be observed in **Figure 4.3** (b) and (c). This would be due to the presence of the bimetallic on the ZSM-5 (50) zeolites. Both of NiPd/ZSM-5 (50) and TEOS-NiPd/ZSM-5 (50) catalysts showed highly dispersed nickel particles on the external surface of the support, while the palladium particles was not observed due to the small particles size (Fan *et al.*, 2020), indicating that the TEOS modification on the ZSM-5 (50) had no effect on the bimetallic dispersion. Therefore, the TEOS-modified catalyst had similar Ni (around 10 wt%) and Pd (around 1 wt%) particles dispersion as the unmodified catalyst which was consistent with the results of XRD and XRF analysis.



378235724

CU iThesis 6271009063 thesis / revv: 13092564 11:18:12 / seq: 50

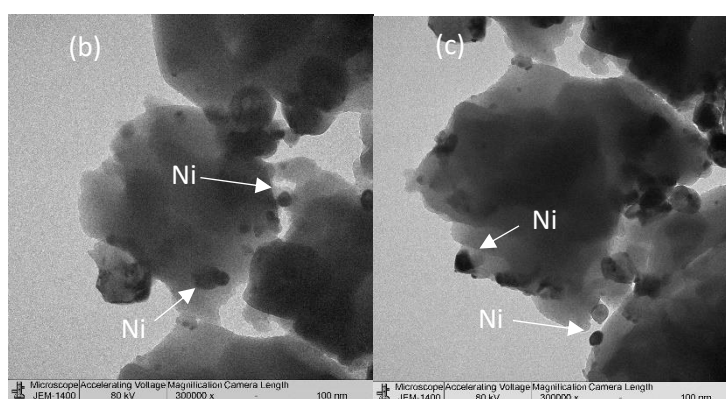
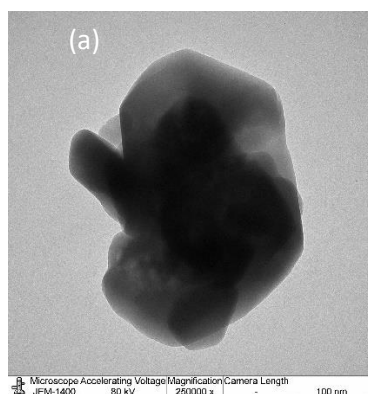


Figure 4.3 TEM images of (a) parent ZSM-5 (50), (b) NiPd/ZSM-5 (50), and (c) TEOS-NiPd/ZSM-5 (50).

4.2 Gas Chromatography of Feed and Standard Analysis

4.2.1 Feed Analysis

The chromatogram and composition of PFAD feedstock analyzed by a GC/FID (Agilent 7890A) are shown in **Figure 4.4** and **Table 4.4**, respectively. The chromatogram of PFAD feedstock showed the main peaks that are hexadecane, octadecane, myristic acid, palmitic acid, oleic acid, stearic acid, mono-glyceride and di-glyceride and triglyceride. The retention times are at 13.759, 15.776, 17.356, 17.7076, 19.810, 20.083, 31-33, 34-36 and 37-38, respectively. Moreover, the compositions of PFAD are shown in **Table 4.4**, it can be revealed that PFAD contains palmitic acid and oleic acid as the main components (46.48% and 43.41%, respectively) and trace amount of hexadecane, octadecane, stearic acid,

mono-glycerides, di-glycerides, and triglycerides.

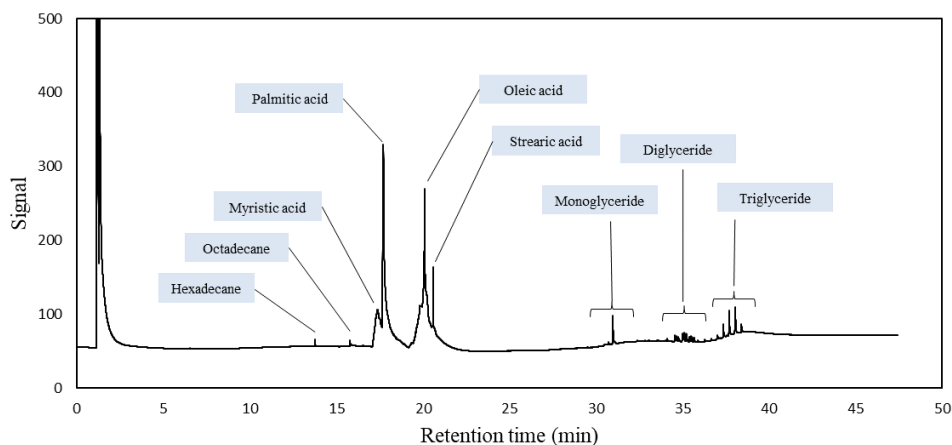


Figure 4.4 The chromatogram of various components in PFAD analyzed by a GC/FID.

Table 4.4 Composition of PFAD feedstock

Feed components	Amount (wt. %)
Palmitic acid	46.48
Oleic acid	43.41
Stearic acid	4.00
Diglycerides	2.28
Mono glyceride	1.45
Octadecane	1.14
Triglyceride	0.86
Hexadecane	0.38

4.2.2 Standard Analysis

The chromatograms of liquid standard were analyzed by gas chromatogram equipped with an FID detector (Agilent 7890A) to identify peaks of the compositions in feedstocks are shown in **Figure 4.5** which are polarity liquid standard (oxygenated compound) consisting of hexadecanol, C20 internal standard, palmitic acid, octadecanol, oleic acid and stearic acid. The retention times are 16.653,

16.939, 17.568, 18.881, 19.808 and 20.293, respectively. Moreover, Figure 6.6 shows non-polarity liquid standard consisting of hexane (C₆), heptane (C₇), octane (C₈), nonane (C₉), decane (C₁₀), dodecane (C₁₂), tetradecane (C₁₄), pentadecane (C₁₅), hexadecane (C₁₆), heptadecane (C₁₇) and octadecane (C₁₈). The retention times are 1.140, 1.203, 1.491, 1.583, 2.204, 6.434, 10.217, 11.595, 12.827, 13.959 and 15.016, respectively. In addition, undecane (C₁₁) and tridecane (C₁₃) had retention times at 2.950 and 8.200.

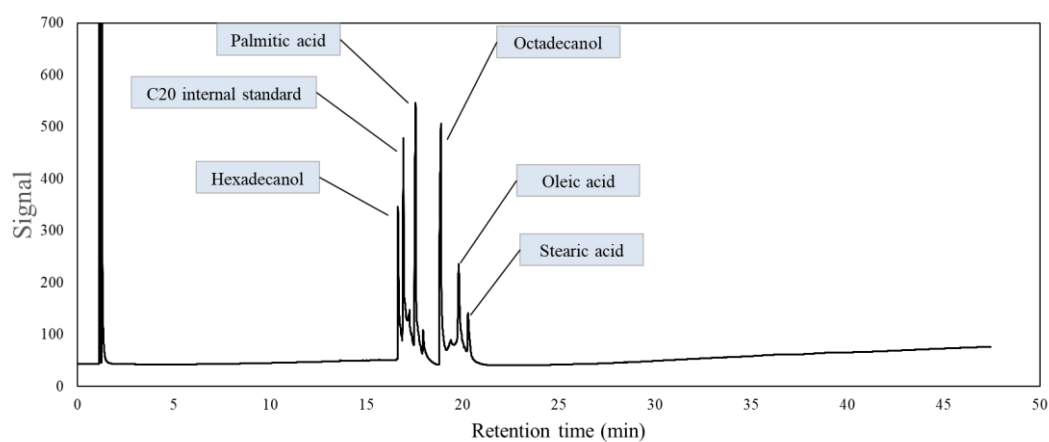


Figure 4.5 Chromatograms of standard oxygenated compounds.

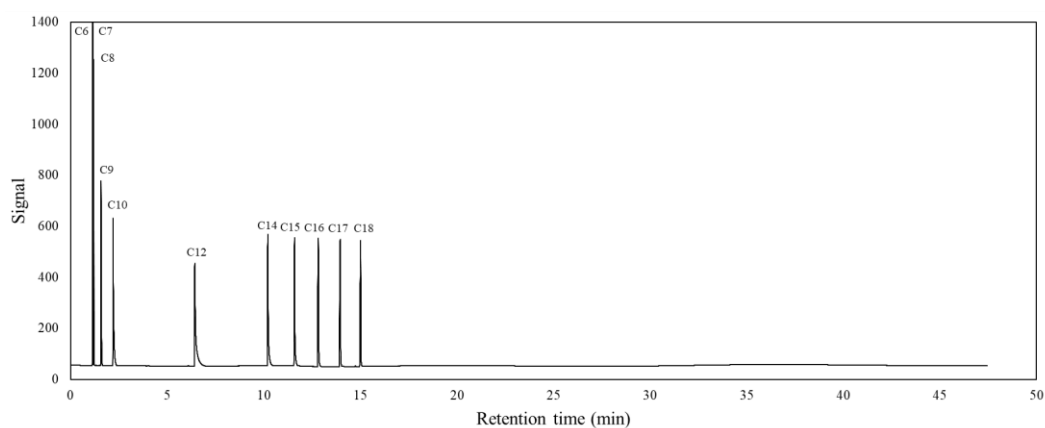


Figure 4.6 Chromatograms of standard n-alkanes.

4.3 Catalytic Activity Testing

In this part, the conversion of PFAD and yield of product over bimetallic NiPd supported on ZSM-5 zeolite with various Si/Al ratios (23, 50, and 280) and modified ZSM-5 zeolites by TEOS were investigated. Moreover, the optimum reaction conditions (temperature and pressure) were also studied.

4.3.1 Effect of the Si/Al Ratios (23, 50, and 280)

Figure 4.7 shows the conversion of PFAD and yields of products over NiPd/ZSM-5 (23), NiPd/ZSM-5 (50), and NiPd/ZSM-5 (280) catalysts at 350 °C, 30 bar, LHSV of 1.5 h⁻¹ and H₂/feed molar ratio of 8. Almost complete conversion was observed for all the catalysts, indicating that the catalyst had a high deoxygenation activity. Moreover, all the catalyst had a high stability corresponding to the previous study (Chen *et al.*, 2016). NiPd/ZSM-5 (23) exhibited the highest yield of light product (around 40%) with low yield of bio-jet fuel (around 25%) since the catalyst had the highest acidity which favored to high hydrocracking. NiPd/ZSM-5 (50) exhibited a lower light product yield of 35.2% at 5 h. After that, the yield remained at around 30% during the process. The bio-jet fuel yield was increased up to 40.8% at 5 h and remained at around 40% during the process. For NiPd/ZSM-5 (280), the high yield of light product was observed at first 5 h. After that, it decreased continuously with increased diesel product yield of 39.1% at 7 h and gave the lowest yield of bio-jet fuel around 10.0%.

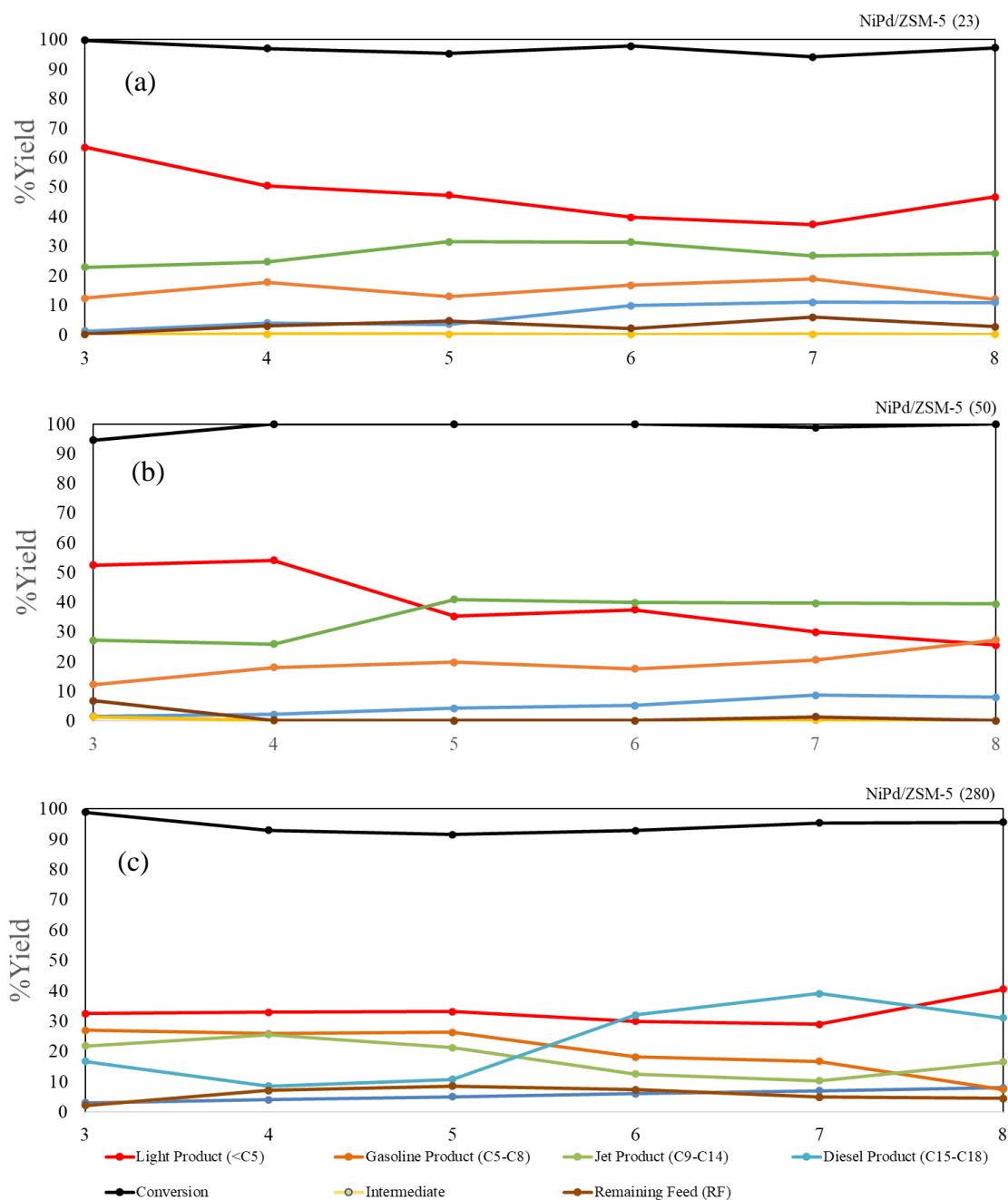


Figure 4.7 PFAD conversion and product yield over (a) NiPd/ZSM-5 (23), (b) NiPd/ZSM-5 (50), and (c) NiPd/ZSM-5 (280) (Reaction condition: 350°C, 30 bar, LHSV = 1.5 h⁻¹, and H₂/feed = 8).

The conversion, product yield, and *iso*-/*n*-paraffin ratio (C₉-C₁₄) obtained over NiPd/ZSM-5 (23), NiPd/ZSM-5 (50), and NiPd/ZSM-5 (280) catalysts at 350 °C, 30 bar, LHSV = 1.5 h⁻¹, H₂/feed molar ratio of 8 and time on stream (TOS)

of 3 h are shown in **Figure 4.8**. NiPd/ZSM-5 (23) had a high acidity that affected excessive cracking thus obtaining high light product yield of 63.5% and gave the low bio-jet fuel yield of 22.8% with *iso-/n*-paraffin ratio (C_9-C_{14}) of 2.77. On the other hand, NiPd/ZSM-5 (280) had a low acidity resulted in low hydrocracking, giving high diesel yield of 16.7% and bio-jet fuel yield of 21.7% with *iso-/n*-paraffin ratio (C_9-C_{14}) of 1.27. NiPd/ZSM-5 (50) gave the highest bio-jet yield of 27.1% *iso-/n*-paraffin ratio (C_9-C_{14}) of 1.82. This would be due to its suitable acidity for cracking long hydrocarbon chain to hydrocarbon chain in the range of bio-jet fuel (C_9-C_{14}) (Feng *et al.*, 2020). The results indicated that an increase in Si/Al ratio resulted in a lower acidity. Thus, lowering hydrocracking and isomerization (Rahman *et al.*, 2020).

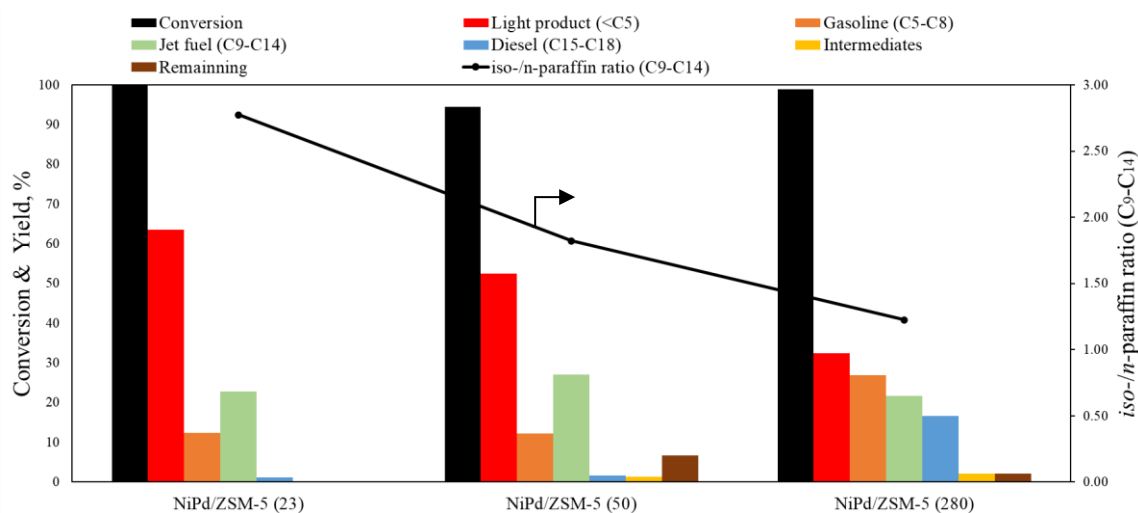


Figure 4.8 PFAD conversion, product yield, and *iso-/n*-paraffin (C_9-C_{14}) over NiPd/ZSM-5 (23), NiPd/ZSM-5 (50), and NiPd/ZSM-5 (280) (Reaction condition: 350°C, 30 bar, LHSV = 1.5 h⁻¹, H₂/feed = 8 and TOS = 3 h).

4.3.2 Effect of TEOS Modification on ZSM-5 Zeolites

The conversion and product yield obtained over NiPd/ZSM-5 (23), TEOS-NiPd/ZSM-5 (23), TEOS (2)-NiPd/ZSM-5 (23), NiPd/ZSM-5 (50), TEOS-NiPd/ZSM-5 (50), NiPd/ZSM-5 (280) and TEOS-NiPd/ZSM-5 (280) catalysts at 350°C, 30 bar, LHSV of 1.5 h⁻¹, H₂/feed molar ratio of 8 and time on stream of 3 h are shown in **Figure 4.9**. All the catalysts gave high conversion of PFAD ($\geq 90\%$). The light product yield of TEOS-NiPd/ZSM-5 (23), TEOS (2)-NiPd/ZSM-5 (23), TEOS-NiPd/ZSM-5 (50), and TEOS-NiPd/ZSM-5 (280) (43.9%, 40.4%, 44.2%, and 28.82%, respectively) was decreased as compared with the unmodified catalyst which were NiPd/ZSM-5 (23), NiPd/ZSM-5 (50), and NiPd/ZSM-5 (280) (63.5%, 52.4%, and 32.42%, respectively). On the other hand, the bio-jet fuel yield of TEOS-NiPd/ZSM-5 (23), TEOS (2)-NiPd/ZSM-5 (23), TEOS-NiPd/ZSM-5 (50), and TEOS-NiPd/ZSM-5 (280) (29.4%, 30.2%, 44.2%, and 30.7%, respectively) was increased as compared with the unmodified catalysts which were NiPd/ZSM-5 (23), NiPd/ZSM-5 (50), and NiPd/ZSM-5 (280) (22.8%, 27.1%, and 21.7%, respectively). These results were similar to their previous study (Zhao *et al.*, 2016) that the TEOS modification mainly affected the external surface by reduced the external Brønsted acid site, especially the strong external Brønsted acid concentration which favored to cracked long chain hydrocarbons to short chain hydrocarbons on the external surface of the catalysts. Therefore, The TEOS-modified catalysts exhibited on lower yield of light product with a higher yield of bio-jet fuel. In addition, the isomerization of the products mainly depended on the internal Brønsted acid site (Feng *et al.*, 2020), so the *iso*-/*n*-paraffin ratio (C₉-C₁₄) of the TEOS-modified catalysts were slightly decreased from the *iso*-/*n*-paraffin ratio (C₉-C₁₄) of the unmodified catalysts. From this results, TEOS-NiPd/ZSM-5 (50) gave the maximum bio-jet fuel yield of 44.2% with the with an *iso*-/*n*-paraffin ratio (C₉-C₁₄) of 1.65.

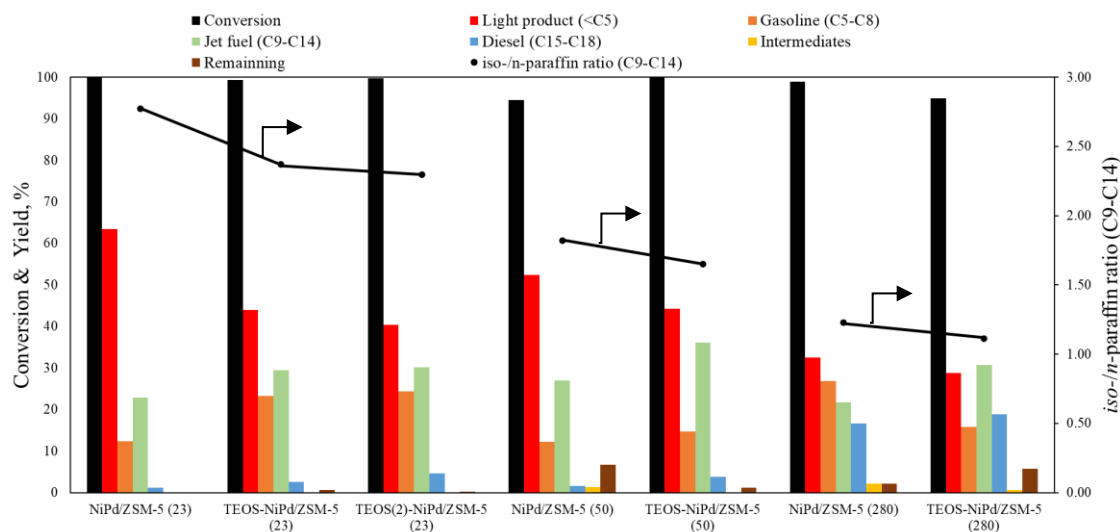


Figure 4.9 PFAD conversion, product yield, and *iso-/n-paraffin* (C₉-C₁₄) over NiPd/ZSM-5 (23), TEOS-NiPd/ZSM-5 (23), TEOS (2)-NiPd/ZSM-5 (23), NiPd/ZSM-5 (50), TEOS-NiPd/ZSM-5 (50), NiPd/ZSM-5 (280), and TEOS-NiPd/ZSM-5 (280) catalysts (Reaction condition: 350 °C, 30 bar, LHSV = 1.5 h⁻¹, H₂/feed = 8 and TOS = 3 h).

4.3.3 Effect of Reaction Temperature

In this part, the effect of the reaction temperature was also studied. **Figure 4.10** shows the conversion, yield of product and *iso-/n-paraffin* ratio (C₉-C₁₄) at reaction temperature 325 °C, 350 °C and 375 °C obtained over TEOS-NiPd/ZSM-5 (50) at 30 bar, LHSV of 1.5 h⁻¹, H₂/feed molar ratio of 8 and time on stream (TOS) of 3 h. The results showed that the reaction temperature at 325-375 °C provided almost complete conversion. The reaction temperature at 375 °C gave highest light product yield of 57.2%. This indicated that high reaction temperature resulted in high hydrocracking of diesel and bio-jet fuel to lighter hydrocarbon products. However, the maximum bio-jet fuel yield of 44.2% with an *iso-/n-paraffin* ratio (C₉-C₁₄) of 1.65 was obtained at 350 °C with completely converting PFAD, since the reaction temperature is suitable cracking the longer chain hydrocarbons into the hydrocarbon range of bio-jet fuel. Therefore, the optimum temperature to convert PFAD to bio-jet fuel is 350 °C (Wei, 1996).



378235724

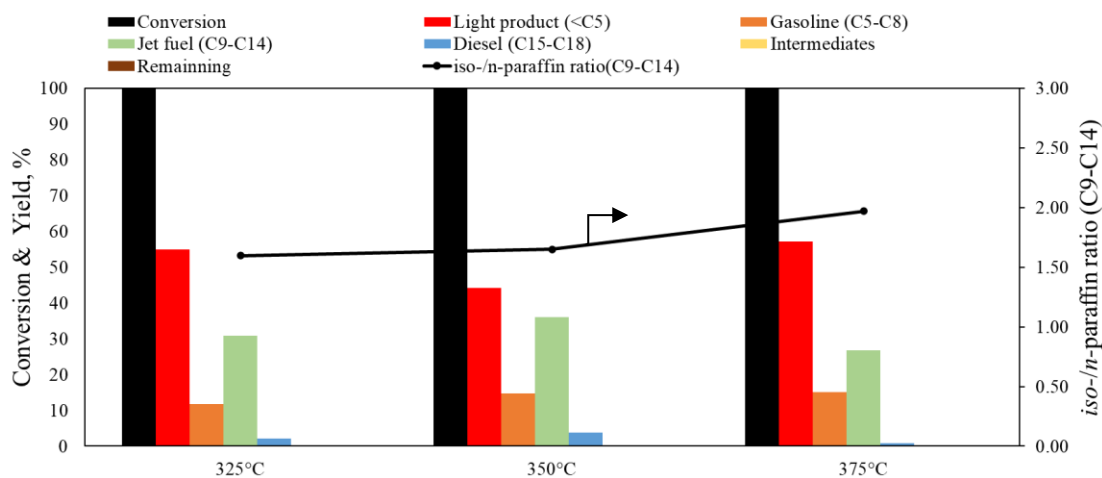


Figure 4.10 PFAD conversion, product yield, and *iso-/n-paraffin* ratio (C₉-C₁₄) over TEOS-NiPd/ZSM-5 (50) with different temperature (Reaction condition: 30 bar, LHSV = 1.5 h⁻¹, H₂/feed molar ratio of 8 and TOS = 3 h).

4.3.4 Effect of Reaction Pressure

In this part, the effect of the reaction temperature was also studied. **Figure 4.11** shows the conversion, yield of product and *iso-/n-paraffin* ratio (C₉-C₁₄) at reaction pressures 10, 20 and 30 bar obtained over TEOS-NiPd/ZSM-5 (50) at 350 °C, LHSV of 1.5 h⁻¹, H₂/feed molar ratio of 8 and time on stream (TOS) of 3 h. The results showed that reaction pressure at 10 bar gave the lowest conversion of PFAD only 88.1%. However, the conversion of PFAD increased to 98.9% and 99.9% while the reaction pressure increased to 20 and 30 bar, respectively. This indicated that the conversion of PFAD increased with reaction pressure. Moreover, the bio-jet fuel yield and *iso-/n-paraffin* (C₉-C₁₄) were also increased with increased reaction pressure and the reaction pressure at 30 bar gave the highest bio-jet fuel yield of 44.2% with *iso-/n-paraffin* ratio (C₉-C₁₄) of 1.65. These results indicated that high reaction pressure supported the adsorption of hydrogen on the active sites, which facilitated for deoxygenation, hydrocracking and isomerization process (Lee and Ihm, 2013).



3782835724

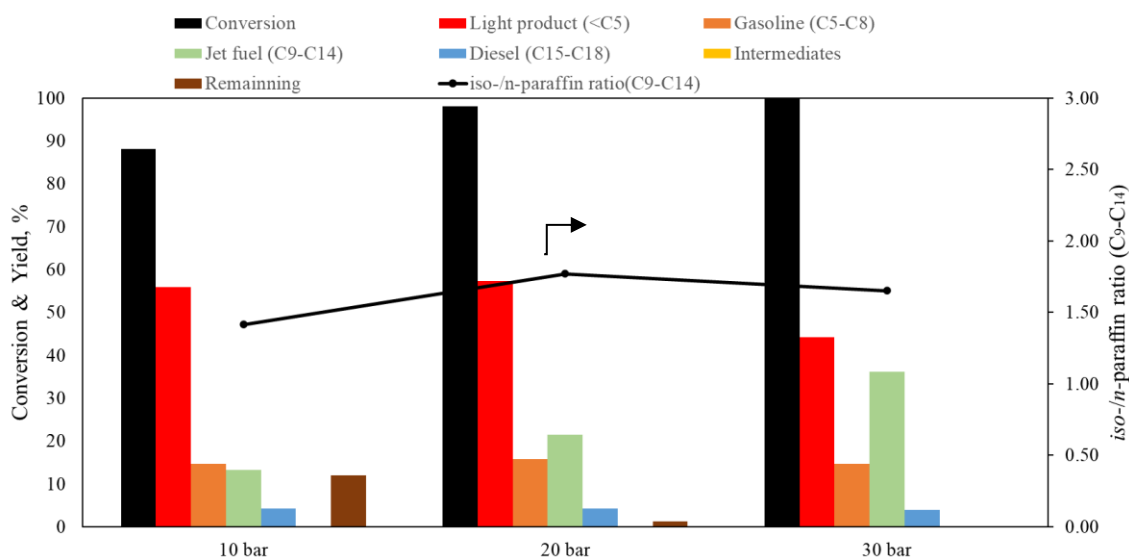


Figure 4.11 PFAD conversion, product yield, and iso-/n-paraffin ratio (C₉-C₁₄) over TEOS-NiPd/ZSM-5 (50) with different pressure (Reaction condition: 350 °C, LHSV = 1.5 h⁻¹, H₂/feed molar ratio of 8 and TOS = 3 h).

4.4 The Proposed Reaction Pathway

Figure 4.12 shows the proposed reaction pathway of palmitic acid which is major component of palm fatty acid distillate. Palmitic acid was converted to a saturated hydrocarbon in the range of diesel by deoxygenation reaction. Deoxygenation is a chemical process including hydrodeoxygenation (HDO), decarboxylation (DCO₂), and decarbonylation (DCO) in which oxygen atoms are removed from fatty acid as H₂O, CO₂, and CO (Silva and De Andrade, 2021). Hydrodeoxygenation reaction (HDO) is process that directs scission of C-O bond to produces a long chain hydrocarbon with the same number of carbon atoms as the fatty acid chain and producing H₂O as a by-product under high hydrogen pressure. Palmitic acid can be converted to hexadecanal via. Then, 1-hexadecanol is produced when hexadecanal is transformed. After that, hexadecane is generated from 1-hexadecanol by dehydrogenation process. Decarbonylation reaction (DCO) refers to removal of carbonyl groups by using hydrogen consumption to produce long chain hydrocarbon with less carbon atoms than fatty acids and CO as a by-product. At first, palmitic acid



is converted to hexadecanal by using hydrogen consumption. Subsequently, hexadecanal is transformed to pentadecane by C-C bond scission, giving CO as a by-product. Moreover, hexadecanal can be transformed to 1-hexadecanol. After that, 1-hexadecanol can also transform to pentadecane through decarbonylation reaction by removing CO and H₂O. Decarboxylation reaction (DCO₂) refers to removal of carboxyl group under hydrogen free atmosphere and directly form pentadecane. Pd is a noble metal which is highly active and selective for the deoxygenation process through decarboxylation pathway (Chen *et al.*, 2018). Moreover, Ni is a non-noble metal selective to decarboxylation pathway and mainly taken part in hydrogenation (Zhang, Chen, *et al.*, 2018). In addition, the hydrocracking reaction is employed to transform long chain hydrocarbons into hydrocarbon in the range of bio-jet fuel by adding hydrogen. On the other hand, the isomerization process converts straight-chain hydrocarbons (*n*-paraffin) to branch-chain hydrocarbons (*i*-paraffin) by removing hydrogen (Wang and Tao, 2016).



378235724

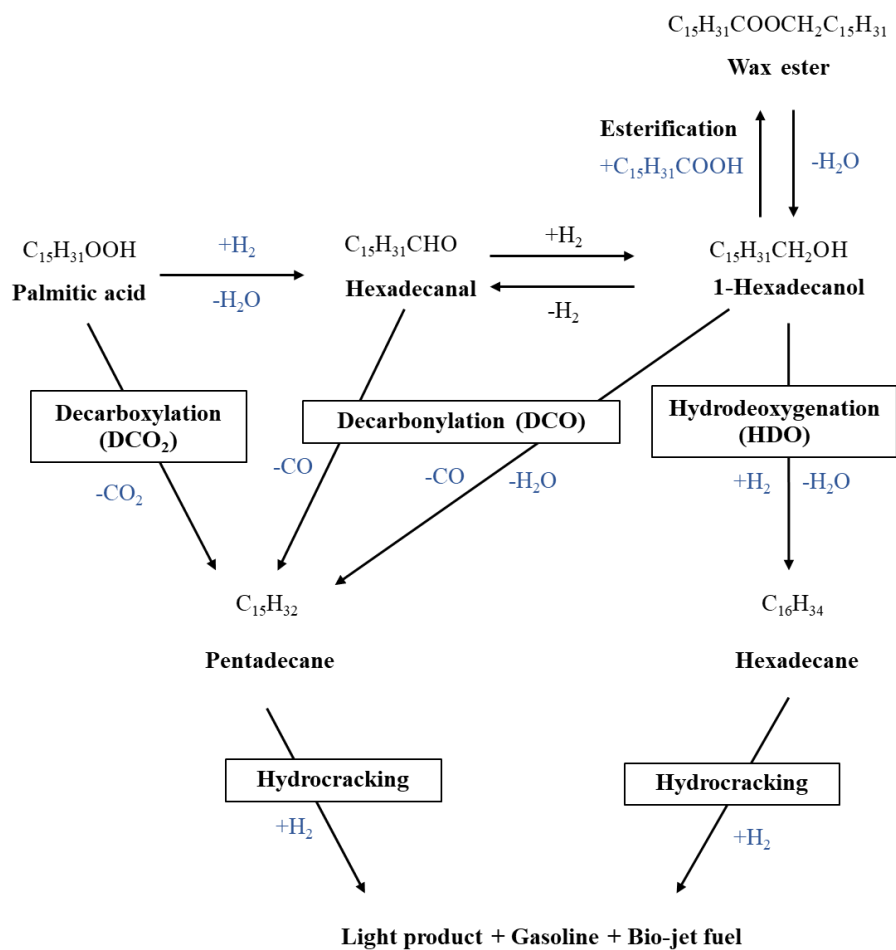


Figure 4.12 The proposed reaction pathway of bio-jet fuel production from palmitic acid over bi-functional catalysts.

CHAPTER 5

CONCLUSIONS AND RECOMMENDATIONS

5.1 Conclusion

In this study, bimetallic (NiPd) supported on ZSM-5 with various Si/Al ratios (23, 50, and 280) and TEOS-modified ZSM-5 zeolites were investigated for the conversion of PFAD to bio-jet fuel. The TEOS-modified catalyst showed similar morphological structure and bimetallic (Ni and Pd) dispersion as compared to the unmodified catalyst, which was confirmed by XRD, XRF, and TEM results. Moreover, after TEOS modification, the Si was on the external surface of the ZSM-5 zeolites was increased, while external Brønsted acid site was decreased, especially the strong external Brønsted acid concentration which favored to cracked long-chain hydrocarbons into short-chain hydrocarbons. NiPd/ZSM-5 (23) had a high acidity, resulting in high light products. NiPd/ZSM-5 (280) exhibited a low acidity, resulting in low hydrocracking, giving high diesel yield. NiPd/ZSM-5 (50) had the highest bio-jet fuel yield of 27.1% as compared to NiPd/ZSM-5 (23) and NiPd/ZSM-5 (280) (22.8% and 21.7%, respectively) due to its suitable acidity for cracking long chain hydrocarbons into the range of bio-jet. Moreover, the TEOS-modified catalyst exhibited lower light product with higher bio-jet fuel as compared to the unmodified catalyst. TEOS-NiPd/ZSM-5 (50) gave the maximum bio-jet fuel yield of 44.2% with an *iso*-/*n*-paraffin ratio (C₉-C₁₄) of 1.65 under the optimum reaction condition at 350 °C, 30 bar, LHSV of 1.5 h⁻¹, and H₂/feed molar ratio of 8.

5.2 Recommendation

To obtain more understanding about the acidity properties of the catalyst, especially on the catalytic cracking, the external Brønsted acid site and Internal Brønsted acid site need to be investigated using TPD and FTIR-pyridine.

In order to improve the bio-jet fuel production from PFAD, acidity of the catalyst should be reduced for prevent high hydrocracking, resulting high light product.

APPENDICES

Appendix A Graphical Abstract

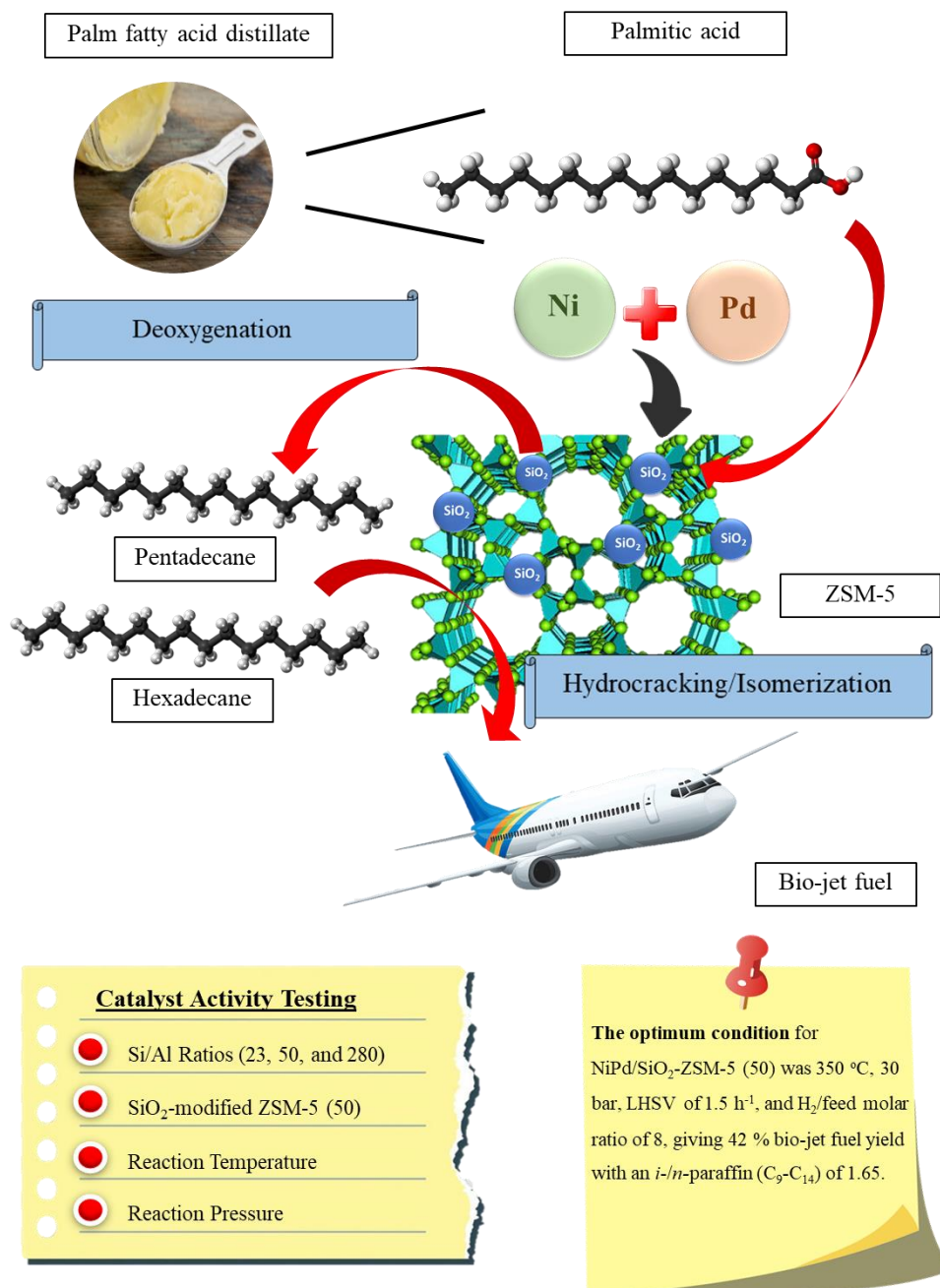


Figure A.1 Graphical Abstract

**Appendix B1 Overall Mass Balance of Deoxygenation-hydroprocessing over
NiPd/ZSM-5 with Various Si/Al Ratio (23, 50, and 280)**

Table B.1 Overall mass balance of deoxygenation-hydroprocessing one-pot reaction over NiPd/ZSM-5 (23), NiPd/ZSM-5 (50), and NiPd/ZSM-5 (280) catalysts (Reaction condition: 350 °C, 30 bar, LHSV of 1.5 h⁻¹, H₂/feed molar ratio of 8, and TOS = 3)

Catalysts		NiPd/ZSM-5 (23)	NiPd/ZSM-5 (50)	NiPd/ZSM-5 (280)
Selectivity of product (wt.%)	C1	6.862	6.548	6.201
	C2	9.300	8.213	2.058
	Ethylene	0.000	0.000	0.000
	C3	24.692	17.343	16.452
	Propylene	0.004	0.014	0.002
	iso-C4	17.024	16.031	2.476
	C4	5.710	7.286	5.662
	iso-C5	0.170	0.518	0.140
	C5	0.022	0.227	0.103
	iso-C6	0.010	0.012	0.000
	C6	0.056	0.006	0.000
	iso-C7	0.000	0.000	0.000
	C7	1.529	4.967	5.109
	iso-C8	0.065	0.459	2.408
	C8	10.555	6.697	19.436
	iso-C9	0.053	15.624	1.920
	C9	10.532	4.697	7.670
	iso-C10	7.803	1.538	5.193
	C10	0.351	3.237	1.806
iso-C11	0.740	0.779	0.329	
C11	0.075	0.021	0.189	

Table B1 (Cont.) Overall mass balance of deoxygenation-hydroprocessing one-pot reaction over NiPd/ZSM-5 (23), NiPd/ZSM-5 (50), and NiPd/ZSM-5 (280) (Reaction condition: 350 °C, 30 bar, LHSV of 1.5 h⁻¹, H₂/feed molar ratio of 8, and TOS = 3 h)

Catalysts		NiPd/ZSM-5 (23)	NiPd/ZSM-5 (50)	NiPd/ZSM-5 (280)
Selectivity of product (wt.%)	iso-C12	1.327	1.493	2.489
	C12	0.032	0.098	0.081
	iso-C13	0.301	0.175	0.442
	C13	0.029	0.071	0.129
	iso-C14	1.583	0.887	1.435
	C14	0.014	0.006	0.297
	iso-C15	0.512	0.537	0.816
	C15	0.116	0.065	2.569
	iso-C16	0.216	0.301	0.846
	C16	0.036	0.032	2.101
	iso-C17	0.162	0.275	2.314
	C17	0.006	0.042	3.885
	iso-C18	0.092	0.376	1.541
C18	0.004	0.055	2.774	
Intermediates		0.064	1.297	1.123
Feed Remaining		2.055	6.729	2.195
% Conversion		98.543	94.568	98.915

**Appendix B2 Overall Mass Balance of Deoxygenation-hydroprocessing at TEOS
modification on ZSM-5 Zeolites**

Table B2 Overall mass balance of deoxygenation-hydroprocessing one-pot reaction over NiPd/ZSM-5 (23), TEOS-NiPd/ZSM-5 (23), TEOS(2)-NiPd/ZSM-5 (23) NiPd/ZSM-5 (50), TEOS-NiPd/ZSM-5 (50), NiPd/ZSM-5 (280), and TEOS-NiPd/ZSM-5 (280) catalysts (Reaction condition: 350 °C, 30 bar, LHSV of 1.5 h⁻¹, H₂/feed molar ratio of 8 and TOS = 3 h)

Catalysts		NiPd/ ZSM-5 (23)	TEOS- NiPd/ ZSM-5 (23)	TEOS (2)- NiPd/ ZSM-5 (23)	NiPd/ ZSM-5 (50)	TEOS- NiPd/ ZSM-5 (50)	NiPd/ ZSM-5 (280)	TEOS- NiPd/ ZSM-5 (280)
Selectivity of product (wt.%)	C1	6.862	3.528	7.376	6.548	6.485	6.201	5.365
	C2	9.300	5.356	1.399	8.213	7.151	2.058	1.022
	Ethylene	0.000	0.002	0.000	0.000	0.000	0.000	0.000
	C3	24.692	23.498	21.230	17.343	17.893	16.452	13.842
	Propylene	0.004	0.026	0.001	0.014	0.000	0.002	0.001
	iso-C4	17.024	6.020	3.896	16.031	5.931	2.476	3.540
	C4	5.710	5.788	6.576	7.286	7.276	5.662	6.597
	iso-C5	0.170	0.057	0.259	0.518	0.670	0.140	0.260
	C5	0.022	0.019	0.085	0.227	0.170	0.103	0.085
	iso-C6	0.010	0.000	0.000	0.012	0.000	0.000	0.000
	C6	0.056	0.000	0.000	0.006	0.000	0.000	0.000
	iso-C7	0.000	0.000	0.000	0.000	0.000	0.000	0.000
	C7	1.529	8.734	5.363	4.967	2.236	5.109	2.265
	iso-C8	0.065	0.138	1.849	0.459	0.170	2.408	0.193
	C8	10.555	14.552	16.913	6.697	11.597	19.436	13.885
	iso-C9	0.053	10.280	17.685	15.624	14.027	1.920	16.567
C9	10.532	8.104	2.910	4.697	10.799	7.670	4.651	
iso-C10	7.803	2.820	3.135	1.538	1.712	5.193	0.803	

Table B2 (Cont.) Overall mass balance of deoxygenation-hydroprocessing one-pot reaction over NiPd/ZSM-5 (23), TEOS-NiPd/ZSM-5 (23), TEOS(2)-NiPd/ZSM-5 (23) NiPd/ZSM-5 (50), TEOS-NiPd/ZSM-5 (50), NiPd/ZSM-5 (280), and TEOS-NiPd/ZSM-5 (280) catalysts (Reaction condition: 350 °C, 30 bar, LHSV of 1.5 h⁻¹, H₂/feed molar ratio of 8 and TOS = 3 h)

Catalysts		NiPd/ ZSM-5 (23)	TEOS -NiPd/ ZSM- 5 (23)	TEOS (2)- NiPd/ ZSM-5 (23)	NiPd/ ZSM-5 (50)	TEOS- NiPd/ ZSM-5 (50)	NiPd/ ZSM-5 (280)	TEOS- NiPd/ ZSM-5 (280)
Selectivity of product (wt.%)	C10	0.351	2.090	2.161	3.237	3.008	1.806	2.498
	iso-C11	0.740	0.985	0.439	0.779	0.959	0.329	0.604
	C11	0.075	0.354	0.163	0.021	0.169	0.189	0.117
	iso-C12	1.327	1.734	1.816	1.493	2.166	2.489	2.336
	C12	0.032	0.011	0.094	0.098	0.024	0.081	0.041
	iso-C13	0.301	0.435	0.417	0.175	0.460	0.442	0.498
	C13	0.029	1.268	0.367	0.071	0.068	0.129	2.089
	iso-C14	1.583	0.652	0.807	0.887	2.038	1.435	1.044
	C14	0.014	0.914	0.289	0.006	1.086	0.297	1.079
	iso-C15	0.512	0.753	0.433	0.537	0.958	0.816	2.308
	C15	0.116	0.313	0.090	0.065	1.086	2.569	4.520
	iso-C16	0.216	0.592	0.487	0.301	0.625	0.846	1.210
	C16	0.036	0.115	0.068	0.032	0.054	2.101	0.808
	iso-C17	0.162	0.462	2.088	0.275	1.022	2.314	3.741
	C17	0.006	0.124	0.459	0.042	0.014	3.885	5.236
	iso-C18	0.092	0.247	1.013	0.376	0.126	1.541	2.052
C18	0.004	0.021	0.074	0.055	0.018	2.774	0.051	
Intermediates		0.065	0.008	0.056	0.029	0.000	5.977	0.694
Feed Remaining		2.055	0.678	0.230	0.010	1.323	6.876	5.995
% Conversion		98.543	99.330	99.771	99.992	98.824	95.786	94.916

Appendix B3 Overall Mass Balance of Deoxygenation-hydroprocessing at Different in Temperature

Table B3 Overall mass balance of deoxygenation-hydroprocessing one-pot reaction over TEOS-NiPd/ZSM-5 (50) catalyst in different temperature (Reaction condition: 30 bar, LHSV of 1.5 h⁻¹, H₂/feed molar ratio of 8 and TOS = 3 h)

Temperature		325 °C	350 °C	375 °C
Selectivity of product (wt.%)	C1	3.543	6.485	8.579
	C2	3.874	7.151	13.077
	Ethylene	0.000	0.000	0.000
	C3	33.241	17.893	24.474
	Propylene	0.029	0.000	0.006
	iso-C4	6.005	5.931	5.791
	C4	8.311	7.276	5.323
	iso-C5	0.459	0.670	0.072
	C5	0.034	0.170	0.010
	iso-C6	0.000	0.000	0.000
	C6	0.000	0.000	0.000
	iso-C7	0.000	0.000	0.000
	C7	2.919	2.236	2.104
	iso-C8	0.612	0.170	0.052
	C8	7.830	11.597	12.961
	iso-C9	10.685	14.027	14.059
	C9	6.926	10.799	4.607
iso-C10	4.209	1.712	1.132	
C10	2.434	3.008	2.662	
iso-C11	1.514	0.959	0.712	

Table B3 (Cont.) Overall mass balance of deoxygenation-hydroprocessing one-pot reaction over NiPd/SiO₂-ZSM-5 (50) catalyst in different temperature (Reaction condition: 30 bar, LHSV of 1.5 h⁻¹, H₂/feed molar ratio of 8 and TOS = 3 h)

Temperature		325 °C	350 °C	375 °C
Selectivity of product (wt.%)	C11	0.462	0.169	0.028
	iso-C12	2.156	2.166	1.541
	C12	0.179	0.024	0.033
	iso-C13	0.701	0.460	0.218
	C13	0.072	0.068	0.037
	iso-C14	1.562	2.038	1.505
	C14	0.025	1.086	0.231
	iso-C15	0.482	0.958	0.270
	C15	0.160	1.086	0.046
	iso-C16	0.638	0.625	0.277
	C16	0.061	0.054	0.012
	iso-C17	0.446	1.022	0.091
	C17	0.078	0.014	0.017
	iso-C18	0.338	0.126	0.060
	C18	0.014	0.018	0.008
Intermediates		0.000	0.000	0.007
Feed Remaining		0.000	1.323	0.006
% Conversion		100.000	98.824	99.99

Appendix B4 Overall Mass Balance of Deoxygenation-hydroprocessing at Different in Pressure

Table B.4 Overall mass balance of deoxygenation-hydroprocessing one-pot reaction over NiPd/SiO₂-ZSM-5 (50) catalyst in different pressure (Reaction condition: 350 °C, LHSV of 1.5 h⁻¹, H₂/feed molar ratio of 8 and TOS = 3 h)

Pressure		10 bar	20 bar	30 bar
Selectivity of product (wt.%)	C1	5.206	9.096	6.485
	C2	11.044	6.743	7.151
	Ethylene	0.011	0.000	0.000
	C3	38.660	27.342	17.893
	Propylene	0.106	0.007	0.000
	iso-C4	12.752	6.658	5.931
	C4	14.576	8.135	7.276
	iso-C5	4.506	2.359	0.670
	C5	1.297	0.982	0.170
	iso-C6	0.000	0.000	0.000
	C6	0.000	0.000	0.000
	iso-C7	0.000	0.000	0.000
	C7	0.000	2.368	2.236
	iso-C8	0.000	0.052	0.170
	C8	0.000	10.229	11.597
	iso-C9	3.538	9.924	14.027
	C9	0.986	3.214	10.799
	iso-C10	0.546	0.838	1.712
	C10	0.797	2.197	3.008
iso-C11	0.234	0.563	0.959	
C11	0.092	0.046	6.485	

Table B4 (Cont.) Overall mass balance of deoxygenation-hydroprocessing one-pot reaction over NiPd/SiO₂-ZSM-5 (50) catalyst in different pressure (Reaction condition: 350 °C, LHSV of 1.5 h⁻¹, H₂/feed molar ratio of 8 and TOS = 6 h)

Pressure		10 bar	20 bar	30 bar
Selectivity of product (wt.%)	iso-C12	0.878	1.524	0.169
	C12	0.101	0.206	2.166
	iso-C13	0.161	0.329	0.024
	C13	0.022	1.231	0.460
	iso-C14	1.160	0.842	0.068
	C14	0.455	0.736	2.038
	iso-C15	0.602	1.367	1.086
	C15	0.138	0.199	0.958
	iso-C16	0.589	0.818	1.086
	C16	0.057	0.094	0.625
	iso-C17	0.637	0.870	0.054
	C17	0.107	0.332	1.022
	iso-C18	0.625	0.546	0.014
	C18	0.049	0.073	0.126
Intermediates		0.067	0.079	0.018
Feed Remaining		0.252	2.647	0.000
% Conversion		88.400	98.990	1.323



378235724

REFERENCES

- Basir, N.M., Jamil, N.A.M., and Hamdan, H. (2021). Conversion of jet biofuel range hydrocarbons from palm oil over zeolite hybrid catalyst. Nanomaterials and Nanotechnology, 11, 1847980420981536.
- Blakey, S., Rye, L., and Wilson, C.W. (2011). Aviation gas turbine alternative fuels: A review. Proceedings of the Combustion Institute, 33(2), 2863-2885.
- Chen, H., Zhang, X., Zhang, J., and Wang, Q. (2018). Tuning the decarboxylation selectivity for deoxygenation of vegetable oil over Pt–Ni bimetal catalysts via surface engineering. Catalysis Science & Technology, 8(4), 1126-1133.
- Chen, L., Li, H., Fu, J., Miao, C., Lv, P., and Yuan, Z. (2016). Catalytic hydroprocessing of fatty acid methyl esters to renewable alkane fuels over Ni/HZSM-5 catalyst. Catalysis Today, 259, 266-276.
- Cheng, J., Li, T., Huang, R., Zhou, J., and Cen, K. (2014). Optimizing catalysis conditions to decrease aromatic hydrocarbons and increase alkanes for improving jet biofuel quality. Bioresource Technology, 158, 378-382.
- De Lucas, A., Sánchez, P., Fúnez, A., Ramos, M., and Valverde, J. (2006). Influence of clay binder on the liquid phase hydroisomerization of n-octane over palladium-containing zeolite catalysts. Journal of Molecular Catalysis A: Chemical, 259(1-2), 259-266.
- Fahim, M.A., Al-Sahhaf, T.A., and Elkilani, A. (2009). Fundamentals of Petroleum Refining, Elsevier.
- Fan, C., Yang, L., Luo, L., Wu, Z., Qin, Z., Zhu, H., Fan, W., and Wang, J. (2020). A highly active Pd/H-ZSM-5 catalyst in lean methane combustion prepared via a sol–gel method and treated by reduction–oxidation. New Journal of Chemistry, 44(10), 3940-3949.
- Galadima, A., and Muraza, O. (2015). Catalytic upgrading of vegetable oils into jet fuels range hydrocarbons using heterogeneous catalysts: A review. Journal of Industrial and Engineering Chemistry, 29, 12-23.
- Hou, X., Qiu, Y., Zhang, X., and Liu, G. (2016). Catalytic cracking of n-pentane over CLD modified HZSM-5 zeolites. RSC advances, 6(59), 54580-54588.
- Ju, C., Zhou, Y., He, M., Wu, Q., and Fang, Y. (2016). Improvement of selectivity from lipid to jet fuel by rational integration of feedstock properties and catalytic strategy. Renewable Energy, 97, 1-7.
- Kallio, P., Pásztor, A., Akhtar, M.K., and Jones, P.R. (2014). Renewable jet fuel. Current Opinion in Biotechnology, 26, 50-55.
- Khan, S., Lup, A.N.K., Qureshi, K.M., Abnisa, F., Daud, W.M.A.W., and Patah, M.F.A. (2019). A review on deoxygenation of triglycerides for jet fuel range hydrocarbons. Journal of Analytical and Applied Pyrolysis, 140, 1-24.
- Kiatkittipong, W., Phimsen, S., Kiatkittipong, K., Wongsakulphasatch, S., Laosiripojana, N., and Assabumrungrat, S. (2013). Diesel-like hydrocarbon production from hydroprocessing of relevant refining palm oil. Fuel Processing Technology, 116, 16-26.
- Lai, Q., Zhang, C., and Holles, J.H. (2016). Hydrodeoxygenation of guaiacol over Ni@Pd and Ni@Pt bimetallic overlayer catalysts. Applied Catalysis A: General,

- 528, 1-13.
- Lee, S.-W., and Ihm, S.-K. (2013). Characteristics of magnesium-promoted Pt/ZSM-23 catalyst for the hydroisomerization of n-hexadecane. Industrial & Engineering Chemistry Research, 52(44), 15359-15365.
- Lestari, S., Mäki-Arvela, P., Beltramini, J., Lu, G.M., and Murzin, D.Y. (2009). Transforming triglycerides and fatty acids into biofuels. ChemSusChem: Chemistry & Sustainability Energy & Materials, 2(12), 1109-1119.
- Malvade, A.V., and Satpute, S.T. (2013). Production of Palm fatty acid distillate biodiesel and effects of its blends on performance of single cylinder diesel engine. Procedia Engineering, 64, 1485-1494.
- Mohammad, M., Hari, T.K., Yaakob, Z., Sharma, Y.C., and Sopian, K. (2013). Overview on the production of paraffin based-biofuels via catalytic hydrodeoxygenation. Renewable and Sustainable Energy Reviews, 22, 121-132.
- Ong, H., Mahlia, T., Masjuki, H., and Norhasyima, R. (2011). Comparison of palm oil, *Jatropha curcas* and *Calophyllum inophyllum* for biodiesel: a review. Renewable and Sustainable Energy Reviews, 15(8), 3501-3515.
- Pattanaik, B.P., and Misra, R.D. (2017). Effect of reaction pathway and operating parameters on the deoxygenation of vegetable oils to produce diesel range hydrocarbon fuels: A review. Renewable and Sustainable Energy Reviews, 73, 545-557.
- Peng, B., Yao, Y., Zhao, C., and Lercher, J.A. (2012). Towards quantitative conversion of microalgae oil to diesel-range alkanes with bifunctional catalysts. Angewandte Chemie International Edition, 51(9), 2072-2075.
- Rahman, M., Infantes-Molina, A., Hoffman, A.S., Bare, S.R., Emerson, K.L., and Khatib, S.J. (2020). Effect of Si/Al ratio of ZSM-5 support on structure and activity of Mo species in methane dehydroaromatization. Fuel, 278, 118290.
- Rai, M., and Da Silva, S.S. (2017). Nanotechnology for Bioenergy and Biofuel Production, Springer.
- Ramsay, J., and Kallus, S. (2000). Zeolite Membranes. Membrane Science and Technology, Elsevier. 6: 373-395.
- Santillan-Jimenez, E., and Crocker, M. (2012). Catalytic deoxygenation of fatty acids and their derivatives to hydrocarbon fuels via decarboxylation/decarbonylation. Journal of Chemical Technology & Biotechnology, 87(8), 1041-1050.
- Scherzer, J., and Gruia, A.J. (1996). Hydrocracking Science and Technology, Crc Press.
- Shahinuzzaman, M., Yaakob, Z., and Ahmed, Y. (2017). Non-sulphide zeolite catalyst for bio-jet-fuel conversion. Renewable and Sustainable Energy Reviews, 77, 1375-1384.
- Silva, G.C.R., and de Andrade, M.H.C. (2021). Simulation of deoxygenation of vegetable oils for diesel-like fuel production in continuous reactor. Biomass Conversion and Biorefinery, 1-15.
- Silva, L.N., Fortes, I.C., de Sousa, F.P., and Pasa, V.M. (2016). Biokerosene and green diesel from macauba oils via catalytic deoxygenation over Pd/C. Fuel, 164, 329-338.
- Silva, L.S.d., Araki, C.A., Marcucci, S.M.P., Silva, V.L.d.S.T.d., and Arroyo, P.A. (2019). Desilication of ZSM-5 and ZSM-12 zeolites with different crystal sizes: effect on acidity and mesoporous initiation. Materials Research, 22.
- Srifa, A., Faungnawakij, K., Itthibenchapong, V., Viriya-Empikul, N., Charinpanitkul,

- T., and Assabumrungrat, S. (2014). Production of bio-hydrogenated diesel by catalytic hydrotreating of palm oil over NiMoS₂/γ-Al₂O₃ catalyst. Bioresource Technology, 158, 81-90.
- Srivastava, N., and Srivastava, P. (2010). Realizing NiO nanocrystals from a simple chemical method. Bulletin of Materials Science, 33(6), 653-656.
- Veriansyah, B., Han, J.Y., Kim, S.K., Hong, S.-A., Kim, Y.J., Lim, J.S., Shu, Y.-W., Oh, S.-G., and Kim, J. (2012). Production of renewable diesel by hydroprocessing of soybean oil: Effect of catalysts. Fuel, 94, 578-585.
- Wang, W.-C., and Tao, L. (2016). Bio-jet fuel conversion technologies. Renewable and Sustainable Energy Reviews, 53, 801-822.
- Wei, J. (1996). Adsorption and cracking of n-alkanes over ZSM-5: negative activation energy of reaction. Chemical Engineering Science, 51(11), 2995-2999.
- Yang, J., Xin, Z., Corscadden, K., and Niu, H. (2019). An overview on performance characteristics of bio-jet fuels. Fuel, 237, 916-936.
- Zhang, C., Hui, X., Lin, Y., and Sung, C.-J. (2016). Recent development in studies of alternative jet fuel combustion: Progress, challenges, and opportunities. Renewable and Sustainable Energy Reviews, 54, 120-138.
- Zhang, D., Wang, Y., and Yang, R.T. (2018). Chemical Liquid Deposition (CLD)-Modified Fe-ZSM-5 for Enhanced Activity and Resistance to C₃H₆ Poisoning in Selective Catalytic Reduction with NH₃ (NH₃-SCR). Industrial & Engineering Chemistry Research, 57(40), 13586-13590.
- Zhang, H., Shao, S., Luo, M., and Xiao, R. (2017). The comparison of chemical liquid deposition and acid dealumination modified ZSM-5 for catalytic pyrolysis of pinewood using pyrolysis-gas chromatography/mass spectrometry. Bioresource Technology, 244, 726-732.
- Zhang, J., and Zhao, C. (2016). Development of a bimetallic Pd-Ni/HZSM-5 catalyst for the tandem limonene dehydrogenation and fatty acid deoxygenation to alkanes and arenes for use as biojet fuel. ACS Catalysis, 6(7), 4512-4525.
- Zhang, T., Shi, J., Liu, J., Wang, D., Zhao, Z., Cheng, K., and Li, J. (2016). Enhanced hydrothermal stability of Cu-ZSM-5 catalyst via surface modification in the selective catalytic reduction of NO with NH₃. Applied Surface Science, 375, 186-195.
- Zhang, Z., Chen, Z., Gou, X., Chen, H., Chen, K., Lu, X., Ouyang, P., and Fu, J. (2018). Catalytic decarboxylation and aromatization of oleic acid over Ni/AC without an added hydrogen donor. Industrial & Engineering Chemistry Research, 57(25), 8443-8448.
- Zhao, Y.-w., Shen, B.-x., and Sun, H. (2016). Chemical liquid deposition modified ZSM-5 zeolite for adsorption removal of dimethyl disulfide. Industrial & Engineering Chemistry Research, 55(22), 6475-6480.
- CEIC. (2021). Malaysia Palm Fatty Acid Distillate Export Price. Retrieved from <https://www.ceicdata.com/en/malaysia/palm-oil-price/palm-fatty-acid-distillate-export-price-fob>

VITA

NAME	Umbon Boonsard
DATE OF BIRTH	2 February 1997
PLACE OF BIRTH	Songkhla
INSTITUTIONS ATTENDED	2019-2020 Master of Science in Petrochemical Technology, The Petroleum and Petrochemical College, Chulalongkorn University, Bangkok, Thailand. 2015-2018 Bachelor of Engineering in Petrochemical and Polymeric material, Faculty of Engineering and Technology, Silpakorn University.
HOME ADDRESS	654 Leabkhongchonlaprathan road City Hatyai Stat Songkhla Postcode 90110 Country Thailand